Polymer Crystallization Driven by Anisotropic Interactions

CHAPTER in ADVANCES IN POLYMER SCIENCE · OCTOBER 2005

Impact Factor: 1.99 · DOI: 10.1007/12_011

2 AUTHORS, INCLUDING:

Daan Frenkel
University of Cambridge
545 PUBLICATIONS **26,638** CITATIONS

SEE PROFILE

Adv Polym Sci (2005) 191: 1–35
DOI 10.1007/12_011

Published online: 5 October 2005

Polymer Crystallization Driven by Anisotropic Interactions

Wenbing Hu[1] (✉) · Daan Frenkel[2]

[1]Department of Polymer Science and Engineering, State Key Lab of Coordination Chemistry, College of Chemistry and Chemical Engineering, Nanjing University, 210093 Nanjing, P.R. China
wbhu@nju.edu.cn

[2]FOM Institute for Atomic and Molecular Physics, Kruislaan 407, 1098 SJ Amsterdam, The Netherlands
frenkel@amolf.nl

Abstract In this review, we consider a variety of aspects of polymer crystallization using a very simple lattice model. This model has three ingredients that give it the necessary flexibility to account for many features of polymer crystallization that have been observed experimentally. These ingredients are (1) a difference in attraction between neighboring (nonbonded) components, (2) attraction between parallel bonds, and (3) temperature-dependent flexibility due to the energy cost associated with kinks in the

polymer chain. We consider this model using both dynamic Monte Carlo simulations and a simple mean-field theory. In particular, we focus on the interplay of polymer crystallization and liquid–liquid demixing in polymer solutions. In addition, we study the factors that are responsible for the characteristic crystal morphologies observed in a variety of homopolymer and statistical-copolymer crystals. Finally, we consider how the freezing of polymers in the bulk can be related to the crystallization of a single polymer chain.

Keywords Crystallization · Lattice statistics · Melting · Monte Carlo simulations · Phase diagram

1 Introduction

The building blocks of liquid-crystalline polymers are anisometric, and many of them form liquid-crystalline mesophases, even in monomeric form. Monomers that have this property are called mesogens. The molecular driving force to form a nematic phase can be due to anisotropic steric repulsions between the anisometric hard cores of the mesogens. This mechanism was proposed by Onsager [1]. It provides a successful description of many lyotropic disorder–order phase transitions. Alternatively, nematic ordering can be induced by the anisotropy of the polarizability of the mesogens, making the parallel orientation of mesogens energetically favorable. This mechanism for the isotropic–nematic transition was proposed by Maier and Saupe [2, 3]. It provides a useful description of thermotropic disorder–order phase transitions. In many cases of practical interest, both interactions play a role and should be taken into account in a description of the isotropic–nematic transition [4–11].

The building blocks of nonmesogenic polymers are also nonspherical; however, their degree of nonsphericity may be insufficient to induce nematic ordering. As already pointed out by Flory [12], the rigidity of a polymer chain – and thereby the anisometry of the Kuhn segments—tends to increase with decreasing temperature. Flory argued (on basis of the Onsager model) that, at sufficiently low temperatures, the anisometry of the Kuhn segments becomes so large that the isotropic (disordered) state is no longer stable and spontaneous ordering—in this case crystallization—must occur [12]. Note that this freezing mechanism is rather different from the one considered in simple liquids: there it is assumed that freezing occurs simply because the molecules can pack more densely in the solid state than in the liquid. The density change on freezing of simple liquids is typically much less than that observed in the orientational ordering of hard rods. Moreover, most lattice models cannot be used to describe a freezing transition driven by packing alone. However, this does not imply that a lattice model cannot properly describe polymer crystallization other than as an isotropic–nematic transition driven by anisotropic excluded-volume effects. In fact, it is possible to describe polymer freezing by taking into account the enhanced attraction between bonds with parallel orientation.

A lattice model that takes such attractions between parallel bonds into account provides a reasonable prediction of polymer melting points [13] and of their interplay with liquid–liquid demixing in polymer solutions [14]. The same factors that favor freezing do affect to a greater or lesser extent the formation of mesophases; hence, there is a close relation between polymer crystallization and the formation of mesophases, which are frequently observed before polymer crystallization (see other papers in this issue).

In this review, we focus on the effect of anisotropic interactions, in particular parallel attractions, and demonstrate that the inclusion of such interactions in a model leads to a great richness in possible polymer phase behavior. From a practical point of view, the model that we describe has the advantage that it is computationally very cheap—although this advantage comes at the price of sacrificing the greater realism of an off-lattice model.

In what follows, we use simple mean-field theories to predict polymer phase diagrams and then use numerical simulations to study the kinetics of polymer crystallization behaviors and the morphologies of the resulting polymer crystals. More specifically, in the molecular driving forces for the crystallization of statistical copolymers, the distinction of comonomer sequences from monomer sequences can be represented by the absence (presence) of parallel attractions. We also devote considerable attention to the study of the free-energy landscape of single-chain homopolymer crystallites. For readers interested in the computational techniques that we used, we provide a detailed description in the "Appendix."

2
Lattice Model for Polymer Crystallization

2.1
Flory's Treatment for Semiflexible Polymers

The structure of a simple mixture is dominated by the repulsive forces between the molecules [15]. Any model of a liquid mixture and, *a fortiori* of a polymer solution, should therefore take proper account of the configurational entropy of the mixture [16–18]. In the standard lattice model of a polymer solution, it is assumed that polymers "live" on a regular lattice of n sites with coordination number q. If there are n_2 polymer chains, each occupying r consecutive sites, then the remaining n_1 single sites are occupied by the solvent. The total volume of the incompressible solution is $n = n_1 + rn_2$. In the case $r = 1$, the combinatorial contribution of two kinds of molecules to the partition function is

$$Z_{\text{comb}} = \frac{n!}{n_1!n_2!} \approx \left(\frac{n}{n_1}\right)^{n_1} \left(\frac{n}{n_2}\right)^{n_2}. \tag{1}$$

This expression accounts for the configurational entropy of an ideal binary mixture with identical molecular sizes, but not for that of a polymer solution, since polymer chains are large and flexible. For that case, more contributions arise from the chain conformational entropy, first considered by Meyer [19] and then derived by Huggins [20] and Flory [21]. In analogy with a nonreversing random walk on a lattice, the conformational contribution of polymer chains to the partition function is given by

$$Z_{\text{conf}} = \frac{\left(\frac{q}{2}\right)^{n_2} z_c^{(r-2)n_2}}{a^{(r-1)n_2}}, \tag{2}$$

where the first factor 1/2 is the symmetry factor of chain ends. This factor accounts for the fact that the calculation can start from either of two chain ends. In Eq. 2, q is the number of possible ways to put the second chain unit along the chain, z_c $(= q - 1)$ is the number of possible ways to place each subsequent chain unit of the rest, and a is a correction term for each step of random walk due to the presence of other chains. Flory showed that if one assumes random mixing (i.e., ignores all local structural correlations), $a = e$. Huggins used a somewhat more sophisticated procedure to estimate the probability of finding two consecutive vacant sites and obtained the estimate $a = (1 - 2/q)^{-(q/2-1)}$ [22]. To account for semiflexibility, Flory introduced a potential energy penalty E_c for every "kink" in the lattice polymer. The presence of this kink energy changes z_c, the intramolecular part of the partition function, to $z_c = 1 + (q - 2)\exp[-E_c/(k_B T)]$, where k_B is Boltzmann's constant and T the temperature [12]. For the fully disordered state at very high temperatures, the so-called "disorder parameter" d, defined as the mean fraction of consecutive bonds that are not collinear, should be

$$d = \frac{(q-2)\exp\left(-\frac{E_c}{k_B T}\right)}{1 + (q-2)\exp\left(-\frac{E_c}{k_B T}\right)}. \tag{3}$$

As the temperature is decreased, the chains become increasingly rigid: z_c then approaches 1 if we assume that there is only one fully ordered crystalline structure and Z_{conf} for the liquid becomes smaller than 1. This means that, at this level of approximation, the disordered state becomes less favorable than the crystalline ground state. A first-order disorder–order phase transition is expected to occur under these conditions. Flory interpreted this phase transition as the spontaneous crystallization of bulk semiflexible polymers [12]. However, since the intermolecular anisotropic repulsion essential in the Onsager model is not considered in the calculation, only the short-range intramolecular interaction is responsible for this phase transition.

The calculation of Z_{conf} makes use of the random mixing approximation for the fully disordered state. Several authors [23–27] have reported improved estimates of Z_{conf} that take into account the effect of local ordering at low temperatures; however, the resulting improvement in the prediction of the

melting point is not very large [22]. Another approach in the calculation of configurational entropy of semiflexible lattice chains was suggested by DiMarzio [28] and was expanded by Ronca [29], and this has been found useful in the study of orientational relaxation of stretched polymer liquids [30–32].

A number of Monte Carlo simulations have verified the spontaneous disorder–order phase transition of semiflexible polymers in 3D lattice models [33–36]. In molecular dynamics simulations, even the metastable chain-folding in the supercooled melt has been observed [37]. However, the ordering transition studied in these simulations was the one from the isotropic to the nematic phase, rather than the actual crystallization transition [38]. At high densities, cooling results in the formation of a glassy disordered state rather than a crystal [39].

2.2 Implications of Parallel Attractions in Polymer Systems

In Monte Carlo simulations, it has been found that introducing a parallel attraction between the polymer bonds, in addition to the bending-energy penalty, could significantly enhance the first-order nature of the isotropic–nematic phase transition at high concentrations [40, 41]. In fact, the inclusion of attraction between parallel bonds has been found to be useful in many studies of nonmesogenic polymers. Such attractions between parallel bonds can mimic the short-ranged orientational order in polyethylene melts that was observed in molecular dynamics simulations [42], in agreement with experimental observations on *n*-alkane liquids [43]. The anisotropic interactions have been considered in the study of orientational relaxation of stretched polymer melts [30–32] and of local order in polymer networks [44, 45].

An early study on the role of parallel attraction in polymer crystallization was made by Bleha [46], who considered the enthalpic effect of parallel packing on the melting point of polymers. In addition, Mansfield [47] took parallel interactions into account in his Monte Carlo calculation of the chain-folding probability at the interphase zone between lamellar crystals and amorphous liquid. Monte Carlo simulations by Yoon [48] showed that parallel attraction can lead to the formation of ordered domains and a density-functional theory study of melt crystallization by McCoy et al. [49] revealed the existence of an effective "chain straightening force" originating from attractive potentials [50]. In Monte Carlo simulations of AB-copolymer crystallization, parallel attractions were used to distinguish the crystallizable sequences from the noncrystallizable sequences [50–52]. Parallel attractions were also applied in the Monte Carlo study of polymer crystallization from dilute solutions on 2D [53] and 3D lattices [54], as well as from the homopolymer melt in 2D [55] and 3D [56] lattices. In earlier work, we showed that the incorporation of attraction between adjacent, unconnected bonds allows us to reproduce the sectorization of chain-folding in a single lamellar crystal-

lite [57] and the shish-kebab morphology of polymer crystallites induced by a single pre-aligned chain [58]. More details of some simulation results are discussed in Sects. 3 and 4.

2.3 Mean-Field Treatment of Parallel Attractions

We now consider a lattice model for a polymer solution that has both isotropic and anisotropic interactions. A mean-field expression for the free energy of the system can be obtained by approximating the local concentration of polymer chain units by its average value. We consider a solution of polymers consisting of r units on a cubic lattice. The volume fraction occupied by the polymers is denoted by ϕ. Two energetic interaction parameters play a role. One is the "mixing energy" B. It is a measure for the energetic cost (relative to the unmixed situation) for having a solvent particle and a polymer chain unit on adjacent lattice sites: $B = E_{us} - (E_{ss} + E_{uu})/2$, where E_{ab} represents pair interactions of the chain units (u) and the solvent particle (s). The second interaction energy E_p denotes the energy cost to break up a pair of adjacent, parallel polymer bonds. The mixing interactions act between sites and are isotropic, while the parallel attractions act between bonds and are anisotropic.

In the fully disordered state, the probability to find a bond at a given bond site is simply given by the ratio of the total number of bonds $[n_2(r-1)]$ to the total number of bond positions $(nq/2)$. The probability that a given bond has a specific parallel neighbor is therefore given by $2n_2(r-1)/(nq)$. Every bond has $q-2$ neighbors, since two consecutive neighbors along the chain should be subtracted from the coordination number. Unless a neighboring site is occupied by a parallel bond, its energy cost equals E_p. The average potential energy cost due to nonparallel packing is therefore $\ln(z_p) = -1/2(q-2)[1-2n_2(r-1)/(nq)]E_p/(k_BT)$, where the factor $1/2$ eliminates double counting of pair interactions. At the mean-field level, the potential energy due to nonparallel packing reduces the partition function by a factor of $z_p^{n_2(r-1)}$. Similarly, most chain units can have $q-2$ neighbors occupied by solvent. The probability of finding a solvent molecule on a specific neighboring site is n_1/n. It then follows that the total mixing potential energy per chain unit is $\ln(z_m) = -(q-2)n_1B/(nk_BT)$. The corresponding contribution to the partition function is $z_m^{n_2 r}$.

Combining all contributions to the partition function of the disordered state of a lattice polymer solution, we obtain

$$Z = Z_{comb} Z_{conf} z_p^{n_2(r-1)} z_m^{n_2 r} \tag{4}$$
$$= \left(\frac{n}{n_1}\right)^{n_1} \left(\frac{n}{n_2}\right)^{n_2} \left(\frac{q}{2}\right)^{n_2} z_c^{n_2(r-2)} e^{-n_2(r-1)} z_p^{n_2(r-1)} z_m^{n_2 r},$$

where $z_c = 1 + (q-2)\exp\left(-\frac{E_c}{k_B T}\right)$, $z_p = \exp\left\{-\frac{q-2}{2}\left[1 - \frac{2n_2(r-1)}{qn}\right]\frac{E_p}{k_B T}\right\}$, and $z_m = \exp\left[-\frac{(q-2)n_1}{n}\frac{B}{k_B T}\right]$.

The mean-field expression for the free-energy density of the polymer solution is therefore [13, 14]

$$f(\phi) = (1-\phi)\ln(1-\phi) + \frac{\phi}{r}\ln\phi - \phi\ln\left(\frac{qr}{2}\right) - \phi\left[-\left(1-\frac{2}{r}\right)\ln z_c + 1 - \frac{1}{r} + (q-2)B + \frac{q-2}{2}\left(1-\frac{1}{r}\right)E_p\right] - \phi^2\left[(q-2)B + \frac{q-2}{q}\left(1-\frac{1}{r}\right)^2 E_p\right]. \quad (5)$$

In the perfectly ordered crystalline ground state, all polymer bonds are parallel and no solvent–polymer contacts are present. If we ignore disorder (vacancies, kinks) in the polymer crystal at finite temperatures, the free-energy density of the crystalline state is zero.

2.4 Predictions of the Polymer Melting Point

Inspection of the mean-field free-energy density given in the previous paragraph allows us to see the relationship between the (microscopic) molecular parameters of the lattice-polymer model and its (macroscopic) phase diagram. Let us first focus on the equilibrium melting point, i.e., the temperature at which the crystalline phase and the isotropic liquid phase are in thermodynamic equilibrium. We first consider the effect of the energy parameters in the model and of the polymer chain length on the melting point of bulk homopolymers. Polymer solutions and mixtures will be discussed in the next section.

At coexistence, the chemical potentials of given species must be equal. In a plot of $f(\phi)$ versus the polymer concentration ϕ, this equality leads to the familiar common-tangent condition: at coexistence, the tangents to the free-energy densities of the solid and liquid phases must coincide. In the lattice model that we use, the partition function for the fully ordered ground state is given by $Z = 1$ and hence its free-energy density is zero. At finite temperatures, the presence of defects will change the free-energy density of the solid. We ignore this effect. In addition, the lattice model ignores the effect of the vibrational degrees of freedom of the polymers.

In a pure homopolymer system, the free-energy density only depends on E_c (the quantity that determines the chain rigidity) and E_p (the quantity that determines the tendency of backbone chains to form parallel, close-packed structures). Let us first consider the relative stability of the pure polymer melt and the polymer solid in the limit of infinitely long chains. In that case, we

find that the free energies of the liquid and solid are equal when

$$1 + (q-2)\exp\left(-\frac{E_c}{k_B T_m}\right) = \exp\left[1 + \frac{(q-2)^2}{2q}\frac{E_p}{k_B T_m}\right]. \quad (6)$$

If $E_c < k_B T$ at melting, we can ignore the first term on the left-hand side and we obtain

$$T_m = \frac{E_c + \frac{(q-2)^2}{2q}E_p}{k_B[\ln(q-2)-1]}. \quad (7)$$

Equation 7 shows that both an increase in chain rigidity and an increase in the interaction between parallel chains will lead to an increase in the melting point, in agreement with experiments [59–62]. For example, semirigid chains that contain aromatic groups in the chain backbone usually have high melting points. Similarly, aliphatic polyamides that have strong interchain interactions, due to hydrogen bonding, tend to have higher melting points than aliphatic polyesters. In addition, strong interchain interactions are only possible in the absence of steric obstructions. For example, polypropylene has smaller side branches than poly(1-butene) and, *a fortiori*, than poly(1-pentene). And indeed, polypropylene has a higher melting point (460.7 K) compared with poly(1-butene) (411.2 K) and poly(1-pentene) (403.2 K) [63]. Bunn [64] has observed a linear dependence of T_m on the cohesive energy density of the same series of homologues [64]. This observation is understandable because both E_c and E_p contribute to the cohesive energy density of solid polymers in a linear way, and in addition the compounds in the same homologous series should have similar E_c and E_p values.

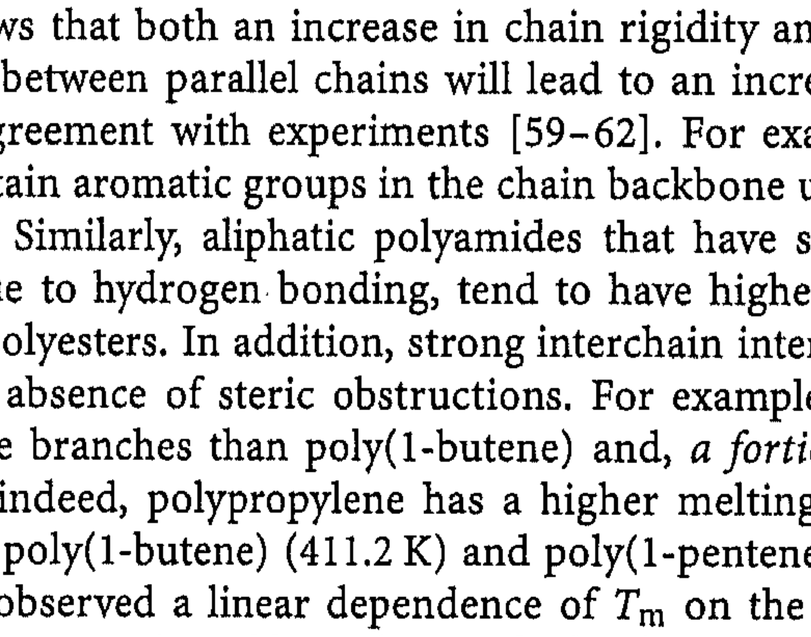

Fig. 1 Melting temperatures of polymers ($k_B T_m/E_c$) with variable E_p/E_c values. The *line* is calculated from Eq. 10 and the *circles* are the simulation results obtained from the onset of crystallization on the cooling curves of disorder parameters, in a short-chain ($r = 32$) system (occupation density is 0.9375 in a 32-sized cubic box) with a template substrate (Hu and Frenkel, unpublished results)

The quality of the mean-field approximation can be tested in simulations of the same lattice model [13]. Ideally, direct free-energy calculations of the liquid and solid phases would allow us to locate the point where the two phases coexist. However, in the present studies we followed a less accurate, but simpler approach: we observed the onset of freezing in a simulation where the system was slowly cooled. To diminish the effect of supercooling at the freezing point, we introduced a terraced substrate into the system to act as a crystallization seed [14]. We verified that this seed had little effect on the phase coexistence temperature. For details, see Sect. A.3. At freezing, we have

$$\mu^{\mathrm{c}} = \mu^{\mathrm{s}}\,, \tag{8}$$

where μ^{c} and μ^{s} are the chemical potentials of the polymers in the crystal and solution, respectively. We ignore disorder in the polymer crystal, so $\mu^{\mathrm{c}} = 0$. As the free-energy expression of the polymer solution is approximated by

$$\begin{aligned}\frac{\Delta F}{k_{\mathrm{B}}T} = \frac{F^{\mathrm{s}}}{k_{\mathrm{B}}T} &= n_1 \ln n_1 + n_2 \ln n_2 - n_1 \ln n - n_2 \ln n - n_2 \ln \frac{q}{2} \\ &\quad + n_2(r-1) - n_2(r-2)\ln z_{\mathrm{c}} \\ &\quad + n_2(r-1)\frac{q-2}{2}\left[1 - \frac{2(r-1)n_2}{qn}\right]\frac{E_{\mathrm{p}}}{k_{\mathrm{B}}T} \\ &\quad + \frac{n_1 n_2 r}{n}\frac{(q-2)B}{k_{\mathrm{B}}T}\,,\end{aligned} \tag{9}$$

the condition that the chemical potentials in the solid and the liquid are equal yields

$$\begin{aligned}&(1-r)\frac{n_2 r}{n} + \ln\frac{qn}{2n_2} + (r-2)\ln\left[1 + (q-2)\exp\left(-\frac{E_{\mathrm{c}}}{k_{\mathrm{B}}T_{\mathrm{m}}}\right)\right] \\ &= \frac{(r-1)(q-2)}{2}\left[1 - \frac{2(r-1)n_2(n+n_1)}{qn^2}\right]\frac{E_{\mathrm{p}}}{k_{\mathrm{B}}T_{\mathrm{m}}} + \frac{rn_1^2}{n^2}\frac{(q-2)B}{k_{\mathrm{B}}T_{\mathrm{m}}}\,.\end{aligned} \tag{10}$$

The melting point T_{m} is computed by solving this equation iteratively. It is often convenient to use $E_{\mathrm{c}}/(k_{\mathrm{B}}T_{\mathrm{m}})$ as our unit of (inverse) temperature. The phase diagram of the polymer solution then depends on the molecular parameters r, q, B/E_{c}, and $E_{\mathrm{p}}/E_{\mathrm{c}}$, the composition parameters n_1 and n_2, and on the temperature parameter $E_{\mathrm{c}}/(k_{\mathrm{B}}T_{\mathrm{m}})$.

Figure 1 shows a comparison of the simulation data with the corresponding theoretical predictions. The figure shows that, over a range of $E_{\mathrm{p}}/E_{\mathrm{c}}$ values, the theoretical predictions are in good agreement with the simulation results. Note that the curve in Fig. 1 is close to the straight line expected on the basis of Eq. 7.

In addition to variations in $E_{\mathrm{p}}/E_{\mathrm{c}}$, we can change the polymer chain length. In particular for small chain lengths, the melting point can be quite sensitive to this parameter [65, 66]. Flory and Vrij [67] analyzed this effect by

treating polymer melting as a virtual two-step process: the first step involves the melting of infinitely long chains and the second step corresponds to the cutting of an infinitely long polymer into chains of finite length. The second step leads to an additional free-energy change Δf_e upon melting, as shown in the equilibrium condition

$$\Delta f_m = r\Delta f_u + \Delta f_e - k_B T_m \ln r = 0\,, \tag{11}$$

where Δf_u is the free-energy change of each chain unit and Δf_e is the additional free-energy change associated with the breakup of the infinite chain. If we assume that the terms in Eq. 7 correspond to the terms in $T_m = \Delta h_u/\Delta s_u$ for each chain unit, we can arrive at the approximate expression

$$\begin{aligned}\Delta f_u =& \Delta h_u - T_m \Delta s_u \\ =& E_c + \frac{(q-2)^2}{2q} E_p - k_B T_m [\ln(q-2) - 1]\,.\end{aligned} \tag{12}$$

The fusion free energy of both chain ends can be calculated from the equilibrium condition $Z = 1$ in Eq. 4 by setting the chain length $r = 2$ in the melt phase. The additional contribution is thus given by

$$\Delta f_e = \frac{(q-2)(q-1)}{2q} E_p - k_B T_m (\ln q - 1) - 2\Delta f_u\,. \tag{13}$$

Figure 2 shows that, for all but the shortest chains, the Flory–Vrij analysis predicts a slightly higher melting temperature than the present mean-field model. Both approximations are give values higher than the simulation results, but the overall agreement is reasonable.

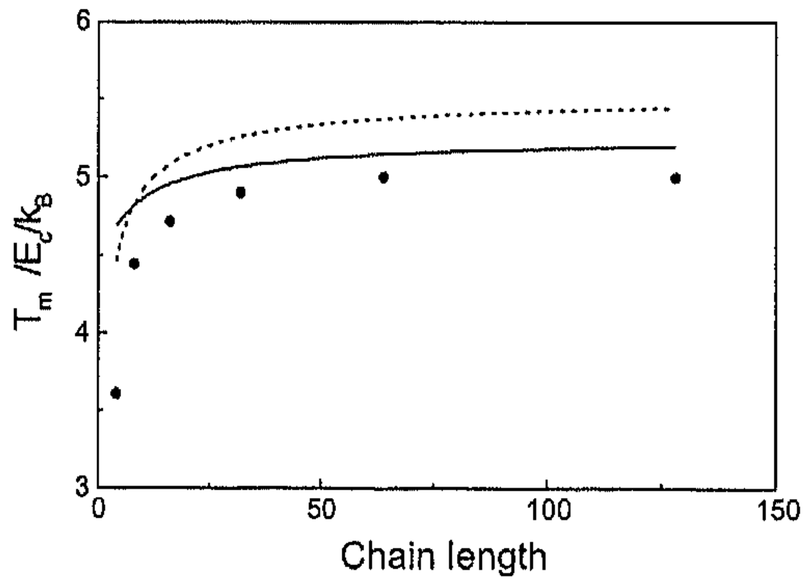

Fig. 2 Melting temperatures of polymers ($k_B T_m/E_c$) with variable chain lengths. The *solid line* is calculated from Eq. 10, the *dashed line* is calculated from Flory–Vrij analysis (Eq. 11), and the *circles* are the simulation results in the optimized approach. In simulations, the occupation density is 0.9375, and the linear size of the cubic box is set to 32 for short chains and 64 for long chains (Hu and Frenkel, unpublished results)

3
Interplay of Polymer Crystallization and Liquid–Liquid Demixing

3.1
Thermodynamic Interplay in Polymer Solutions

When B is positive, the polymer solution can exhibit liquid–liquid demixing. By adjusting the relative values of B and E_p, we can tune the phase diagrams of polymer solutions and study the interplay of freezing, on the one hand, and demixing on the other [14].

To calculate the liquid–liquid coexistence curves, we cast Eq. 5 in the standard Flory–Huggins form where all terms linear in ϕ are subtracted. The free-energy expression then becomes

$$\begin{aligned}\frac{\Delta F_{\mathrm{mix}}}{k_B T} &= n_1 \ln n_1 + n_2 \ln n_2 - n_1 \ln n - n_2 \ln n + n_2 \ln r \\ &\quad + n_2(r-1)\left(\frac{q}{2}-1\right)\frac{2(r-1)}{qr}\left(1-\frac{n_2 r}{n}\right)\frac{E_p}{k_B T} + \frac{n_1 n_2 r}{n}\frac{(q-2)B}{k_B T} \\ &= n_1 \ln \frac{n_1}{n} + n_2 \ln \frac{n_2 r}{n} \\ &\quad + \frac{n_1 n_2 r}{n}\left[\left(1-\frac{2}{q}\right)\left(1-\frac{1}{r}\right)^2 \frac{E_p}{k_B T} + \frac{(q-2)B}{k_B T}\right].\end{aligned} \tag{14}$$

This allows us to introduce an effective χ parameter, through

$$\frac{\Delta F_{\mathrm{mix}}}{k_B T} = n_1 \ln \frac{n_1}{n} + n_2 \ln \frac{n_2 r}{n} + \frac{n_1 n_2 r}{n}\chi_{\mathrm{eff}}, \tag{15}$$

where $\chi_{\mathrm{eff}} = (q-2)B/(k_B T) + (1-2/q)(1-1/r)^2 E_p/(k_B T)$. As usual, the liquid–liquid coexistence curves can be calculated from the chemical-potential equivalence of two mixtures.

Figure 3a shows the mean-field predictions for the polymer phase diagram for a range of values for E_p/E_c and B/E_c. The corresponding simulation results are shown in Fig. 3b. As can be seen from the figure, the mean-field theory captures the essential features of the polymer phase diagram and provides even fair quantitative agreement with the numerical results. A qualitative flaw of the mean-field model is that it fails to reproduce the crossing of the melting curves at $\phi = 0.73$. It is likely that this discrepancy is due to the neglect of the concentration dependence of χ_{eff}. Improved estimates for χ_{eff} at high densities can be obtained from series expansions based on the lattice-cluster theory [68, 69].

Figure 3 illustrates the thermodynamic interplay of polymer crystallization and liquid–liquid demixing in polymer solutions. The liquid–liquid binodal curve is primarily determined by the B value. With the increase of E_p values, the liquid–liquid binodal curves shift slightly upward. On the other hand, the

liquid–solid coexistence curves are primarily controlled by the E_p value. With the decrease of B values from positive to negative, the melting point depression due to dilution will be enhanced. Proper choices of energy parameters can lead to an intersection of two phase-coexistence curves: the phase diagram then exhibits a (monotectic) triple point. Experimental studies of the intersection of freezing and demixing curves in solutions and blends have been reported[70–74].

Flory proposed a semiempirical expression to predict the concentration dependence of the melting curve of long-chain polymers mixed with small solvent molecules [75]:

$$\frac{1}{T_m} - \frac{1}{T_m^0} = \frac{k_B}{\Delta h_u}[1 - \phi - \chi(1-\phi)^2], \tag{16}$$

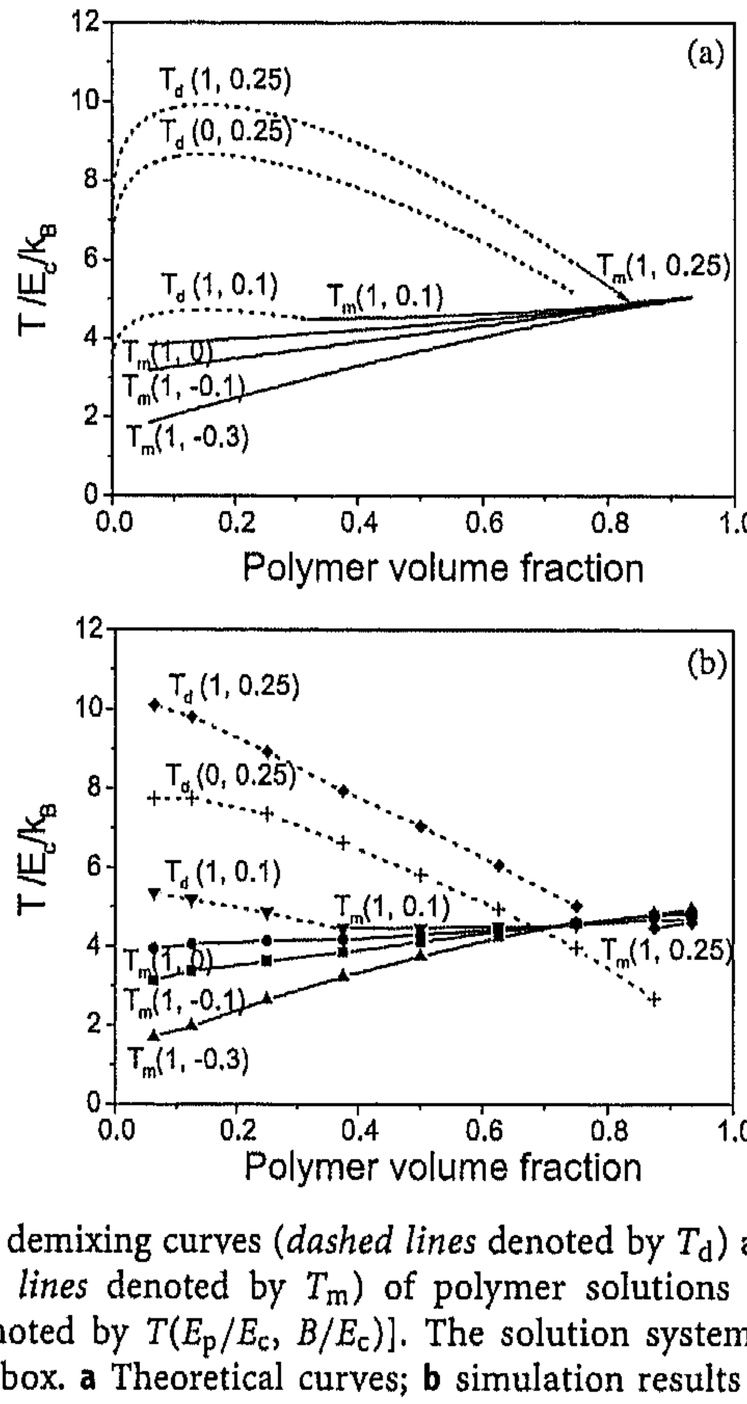

Fig. 3 Liquid–liquid demixing curves (*dashed lines* denoted by T_d) and liquid–solid transition curves (*solid lines* denoted by T_m) of polymer solutions with variable energy parameter sets [denoted by $T(E_p/E_c, B/E_c)$]. The solution system is made of 32-mers in a 32-sized cubic box. **a** Theoretical curves; **b** simulation results in the optimized approach [14]

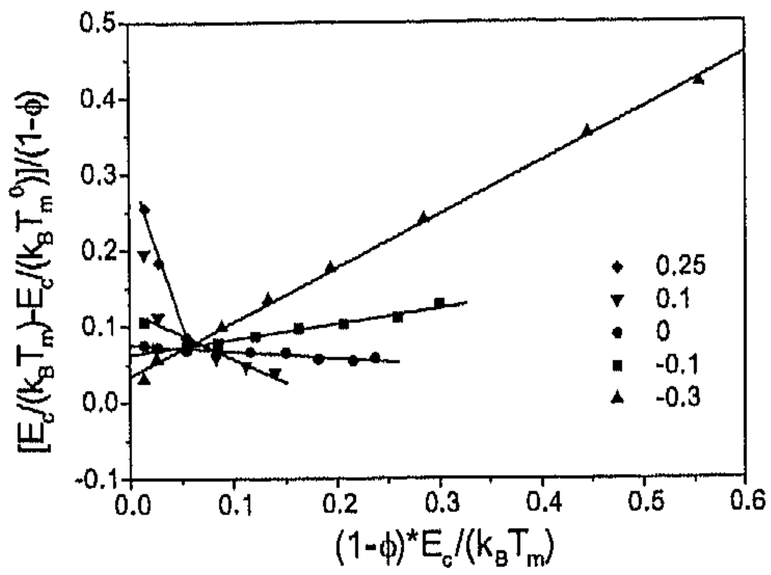

Fig. 4 Rescaled data from Fig. 3b to show the linear relationship predicted by Eq. 16. The bulk equilibrium melting temperature $E_c/k_B T_m^0$ is chosen to be approximately 0.2. The *lines* are the results of linear regression, and the *symbols* are for the variable values of B/E_c [14]

where T_m^0 is the melting point of pure polymers and Δh_u is the heat of fusion per chain unit. This semiempirical equation accounts well for numerous experimental data [76]. In Fig. 4, we have transformed the simulation results of Fig. 3b in such a way that, according to Eq. 16, a linear plot should result. However, the values Δh_u and χ that follow from a fit to the numerical data differ from the expressions that follow from Eq. 16 [14].

3.2 Kinetic Interplay in Polymer Solutions

In the dynamic Monte Carlo simulations described earlier, we used a crystalline template to suppress supercooling (Sect. A.3). If this template is not present, there will be a kinetic interplay between polymer crystallization and liquid–liquid demixing during simulations of a cooling run. In this context, it is of particular interest to know how the crystallization process is affected by the vicinity of a region in the phase diagram where liquid–liquid demixing can occur.

Simulations [77] and theoretical analysis [78, 79] indicate that the rate of homogeneous crystal nucleation may be significantly increased in the one-phase region near a metastable liquid–liquid critical point. In simple polymer solutions and melts, crystallization often occurs after the system has entered the region where fluid–fluid spinodal decomposition takes place. The density modulations that occur during this spinodal decomposition are "frozen in" during subsequent crystallization and affect the morphology of the resulting crystalline phase [80]. This phenomenon is, in fact, of considerable practical importance for the control of sol–gel transitions, in particular in the context of membrane formation [81–83].

To study the interplay between demixing and crystallization, we considered three different model systems, all at a polymer volume fraction of 15% [84]. The interaction parameters of the models were chosen such that all systems had the same (equilibrium) melting temperatures but different demixing temperatures at the chosen concentration. One case (C1) had its critical demixing temperature very close to the melting curve, the second case (C2) had its critical point at a temperature where primary crystal nucleation would occur in the absence of liquid–liquid demixing, and for the third case (C3), the critical demixing temperature was located far below the melting curve. In case C1, we expect to observe demixing prior to crystallization, in case C2 crystallization and liquid–liquid demixing may be strongly coupled, and in case C3, crystal nucleation should proceed without any effect of liquid–liquid demixing. The theoretical (i.e., mean-field) phase diagrams for these three cases are shown in Fig. 5. Figure 6 shows the simulation results for slow cooling runs of homogeneous polymer solutions corresponding to models C1, C2, and C3.

As can be seen from Fig. 6, liquid–liquid demixing clearly precedes crystallization in case C1. Moreover, crystallization in this case occurs at a higher temperature than in cases C2 and C3. Apparently, the crystallization takes place in the dense disordered phase (which has a higher melting temperature than the more dilute solution; Fig. 5). In case C2, the crystallization temperature is close to the expected critical point of liquid–liquid demixing, but higher than in case C3. This suggests that even pre-critical density fluctuations enhance the rate of crystal nucleation.

The different pathways for crystallization have consequences for the resulting crystal morphology. This can be seen in Fig. 7, where we compare the

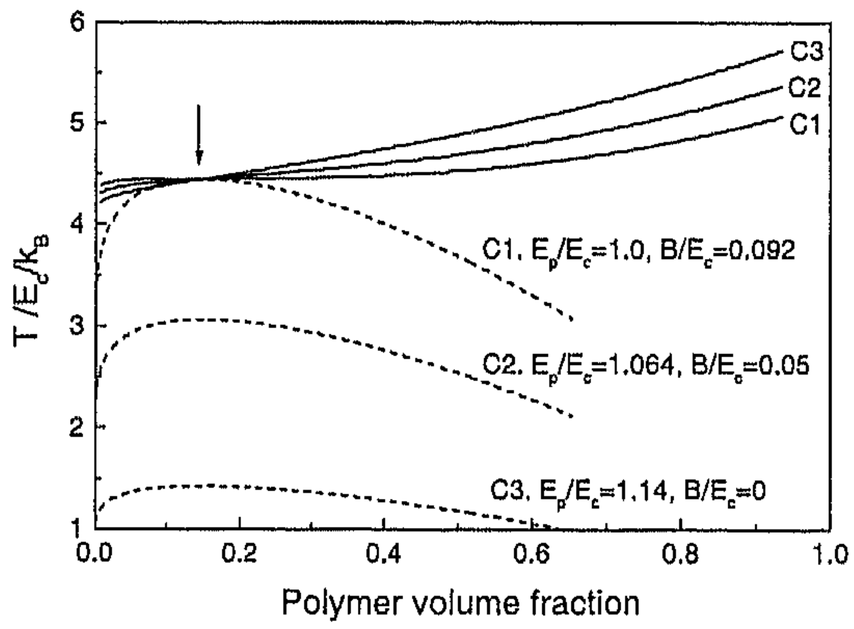

Fig. 5 Theoretical liquid–liquid demixing curves (*dashed lines*) and liquid–solid transition curves (*solid lines*) of 32-mers in a 64-sized cubic box. Three sets of energy parameters are denoted by *C1*, *C2*, and *C3*, respectively. The *arrow* indicates the cooling trajectory of the simulations [84]

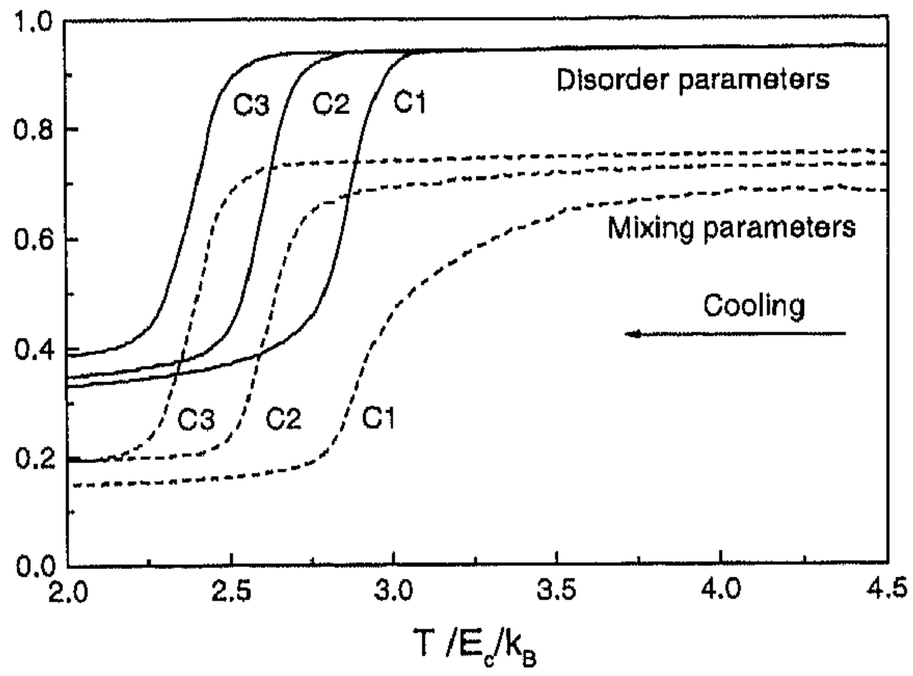

Fig. 6 Simulational cooling curves of disorder parameters (*solid lines*) and mixing parameters (*dashed lines*) for 32-mers with different sets of energy parameters in a 64-sized cubic box (the concentration is fixed at 0.150). The mixing parameter is defined as the mean fraction of neighboring sites occupied by the solvent for each chain unit [84]

crystal morphologies that result if systems C1, C2, and C3 are all quenched to the same temperature ($T = 2.857E_c/k_B$). The figure shows that, for system C1, small crystallites are homogeneously distributed throughout the simulation box. This is the result of liquid–liquid demixing under conditions of a deep spinodal quench (short-wavelength instability), followed by freezing of the high-density domains. In case C2, larger crystallites are formed. This is the result of liquid–liquid demixing under conditions of a shallow spinodal quench (long-wavelength instability), again followed by the freezing of the high-density domains. In case C3, liquid-liquid demixing cannot occur at the

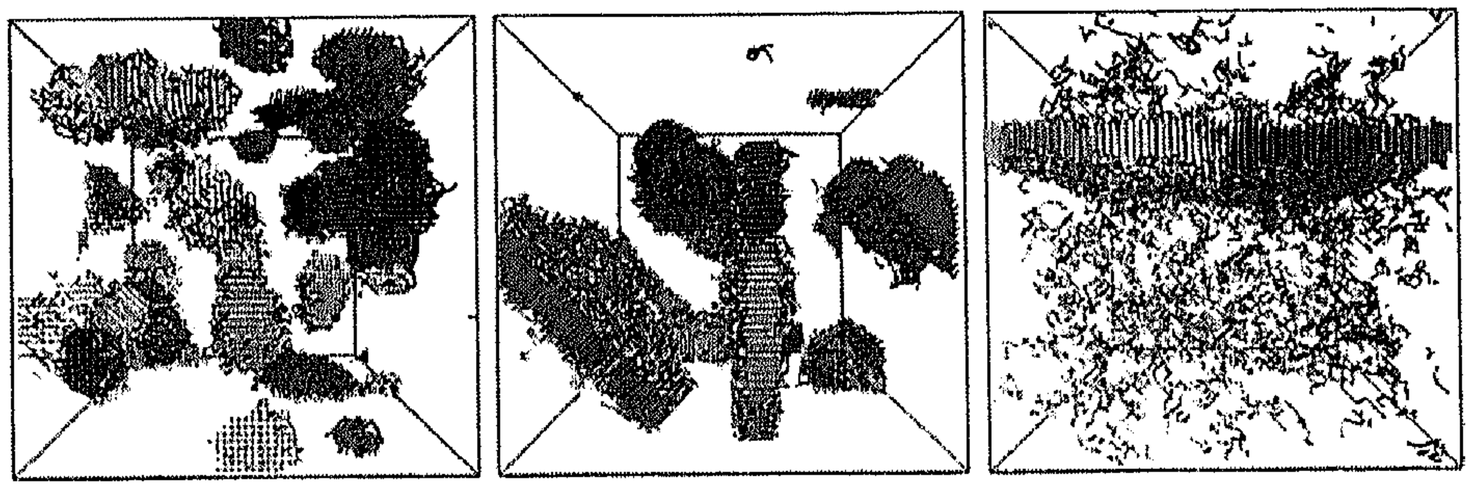

Fig. 7 Snapshots of the simulation systems for C1, C2, and C3 after an isothermal crystallization following the quenching from the infinite temperature to a temperature of 2.857 E_c/k_B [84]

chosen temperature and, indeed, the resulting crystal morphology is quite different: a single, lamellar crystallite grows from the homogeneous solution. For more details on the experimentally observed differences in morphology of polymer crystals grown from solution, the reader is referred to Ref. [85].

3.3 Thermodynamic Interplay of Crystallization and Mixing in Polymer Blends

In polymers mixed with small molecules, there is a very strong entropy penalty for demixing (see Eq. 15). If, in our lattice model, we put B equal to zero and $E_p \neq 0$, polymer crystallization will always pre-empt liquid–liquid demixing (see case C3 in Fig. 5). However, in polymers mixed with long-chain polymers, the entropy penalty for demixing becomes so small that a difference in E_p for the two polymer species may lead to liquid–liquid demixing before crystallization [86]. Recently, the monomeric geometrical assymmetry between two species has been found to raise a positive entropic contribution to the mixing free energy [87]. This was achieved by the lattice-cluster theory with calculations beyond the random mixing approximation [88]. Here, this assymmetry may also be absent for seeing demixing. If we view E_p as a measure for the crystallizability of a polymer, then one could argue that, in such polymer blends, the liquid–liquid demixing is driven solely by the difference in crystallizability of two components [86].

To see this, consider the mixing free energy expression for a polymer blend with symmetrical chain lengths and with only one crystallizable component (i.e., $E_p = 0$ for one component and $E_p \neq 0$ for the other). In that case the (mean-field) partition function for the liquid mixture is

$$Z = \left(\frac{n}{n_1}\right)^{n_1} \left(\frac{n}{n_2}\right)^{n_2} \left(\frac{q}{2}\right)^{n_1+n_2} z_c^{(n_1+n_2)(r-2)} e^{-(n_1+n_2)(r-1)} z_p^{n_2(r-1)} z_m^{n_2 r}, \qquad (17)$$

where z_c and z_p are defined as in Eq. 4, $z_m = \exp\left[-\frac{n_1 r}{n}\frac{(q-2)B}{k_B T}\right]$, n_1 and n_2 denote the number of noncrystallizable and crystallizable polymer chains, all containing r units, $n = n_1 r + n_2 r$, and B is the net potential-energy exchange for a site–site contact between units of types 1 and 2. The mixing free energy of this polymer blend is then

$$\frac{\Delta f_{mix}}{k_B T} = \frac{\phi_1}{r}\ln\phi_1 + \frac{\phi_2}{r}\ln\phi_2 + \phi_1\phi_2\left[(q-2)\frac{B}{k_B T} + \left(1-\frac{2}{q}\right)\left(1-\frac{1}{r}\right)^2 \frac{E_p}{k_B T}\right], \qquad (18)$$

where ϕ_1 and ϕ_2 are the volume fractions of noncrystallizable and crystallizable polymer chains, respectively. When $r \gg 1$, the mixing entropy is very small, and hence a small contribution of E_p may already make the mixed state unstable. Then, liquid–liquid demixing pre-empts polymer crystallization on

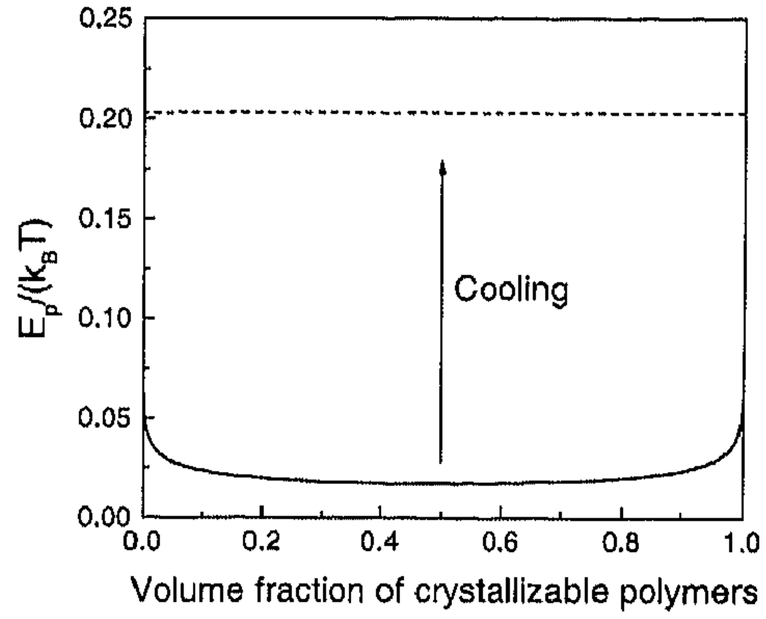

Fig. 8 Theoretical liquid–liquid demixing curve (*solid line*) and the bulk melting temperature (*dashed line*) of a flexible-polymer blend with one component crystallizable and with athermal mixing. The chain lengths are uniform and are 128 units, the linear size of the cubic box is 64, and the occupation density is 0.9375 [86]

cooling (Fig. 8). Such liquid–liquid demixing has been verified by simulation of a cooling process passing through the critical point of the symmetrical-polymer blend [86].

One practical example of demixing that might be attributed to a difference in crystallizability is the incompatibility in blends of polymers with different stereochemical compositions. The stereochemical isomers contain both chemical and geometrical similarities, but differ in the tendency of close packing. In this case, both the mixing energy B and the additional mixing entropy due to structural asymmetry between two kinds of monomers are small. However, the stereochemical differences between two polymers will result in a difference in the value of E_p. Under this consideration, most experimental observations on the compatibility of polymer blends with different stereochemical compositions [89–99] are tractable. For more details, we refer the reader to Ref. [86].

4
Some Applications of Parallel Attractions in Molecular Simulations

4.1
Characteristic Morphologies of Polymer Crystallites

One of the most remarkable features of polymer crystallization is that such chain molecules can form lamellar crystals that contain heavily folded polymer chains. In experiments, the structural analysis of these lamellar crystals became possible when polyethylene single crystals were first prepared from a solution [100–102]. It was found that the orientation of the polymer chains

was perpendicular to the top and bottom faces of the lamellar crystal. However, as the crystal thickness is typically much smaller than the polymer length, this can only be realized if the chains fold back at the top and bottom surfaces. The fold ends prefer to align in parallel to the crystal growth front. However, there is no correlation between the positions of fold ends in successive crystalline layers. During growth, a single crystal can develop several facets. Each facet corresponds to a sector in which the fold ends are preferably parallel to this facet. This leads to the sectorization of chain folding in the single crystal of polymers [103–106]. Interestingly, this sectorization phenomenon can be reproduced in simulations of the simple lattice model described before (Fig. 9) [57]. As in the experiments, we find that the folds are aligned with the growth front but exhibit little correlation from one crystalline layer to the next. The simulations provide molecular-level detail on how a single chain can be incorporated into the growth front. Multiple steps have been found and can be attributed to a limited size of the growth front. A detailed observation of a single chain attaching to the smooth growth front has been reported by Muthukumar's group [107]. There is experimental evidence for sectorization on the surface of thin films of bulk polymers [108, 109]. However, the available simulations have, thus far, not reproduced the sectorization of lamellae grown in the melt away from any surface [56].

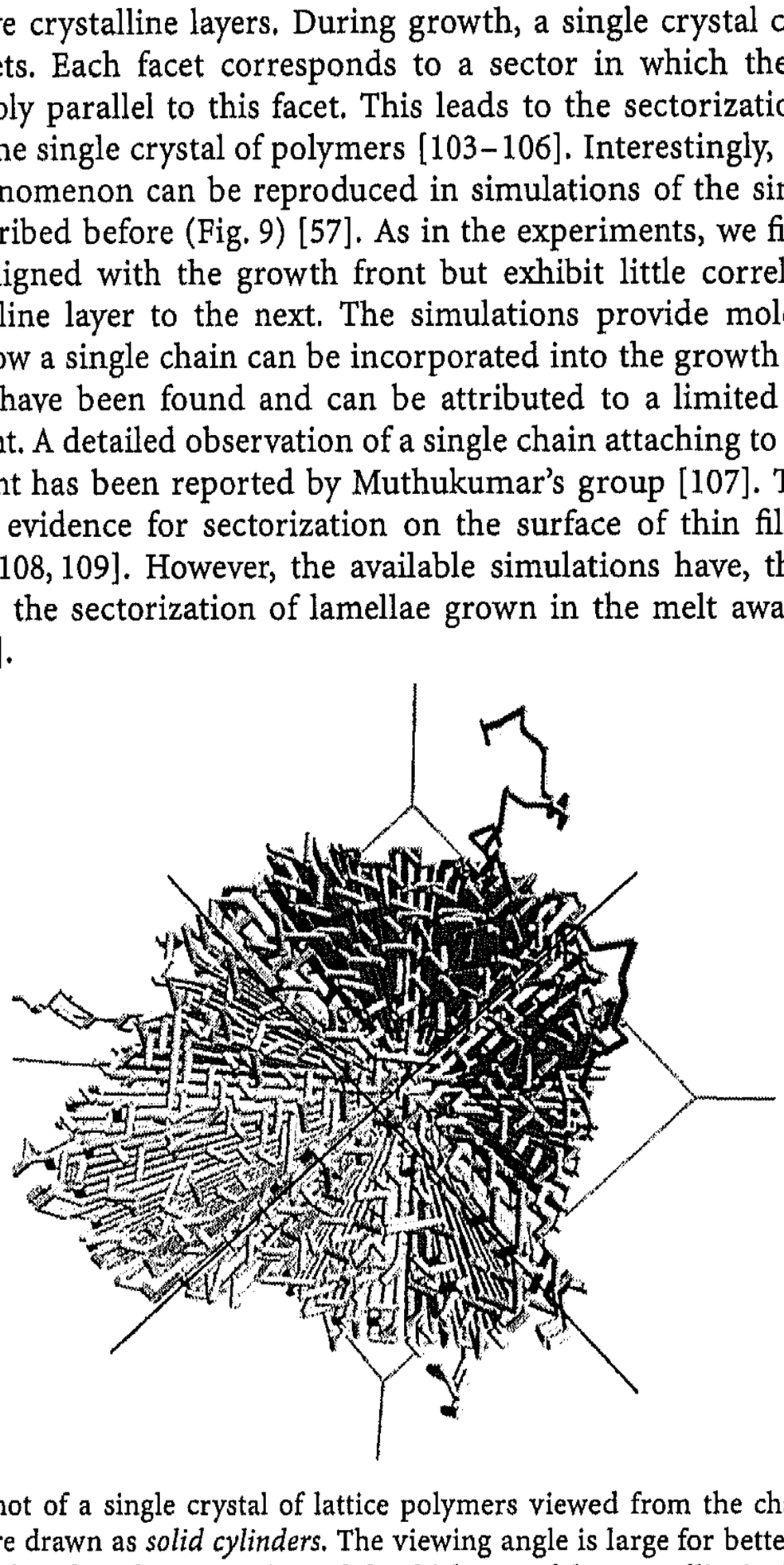

Fig. 9 Snapshot of a single crystal of lattice polymers viewed from the chain direction. The bonds are drawn as *solid cylinders*. The viewing angle is large for better observation of folds. The chain length is 512 units and the thickness of the crystallite is about 12 units. The dissolved chains are not shown for clarity [57]

Polymer crystallization is usually initiated by nucleation. The rate of primary nucleation depends exponentially on the free-energy barrier for the formation of a critical crystal nucleus [110]. If we assume that a polymer crystallite is a cylinder with a thickness l and a radius R, then the free-energy cost associated with the formation of such a crystallite in the liquid phase can be expressed as

$$\Delta F_c(\nu) = -\pi R^2 l|\Delta\mu| + 2\pi R^2\sigma_e + 2\pi Rl\sigma_l\,, \tag{19}$$

where $\nu = \pi R^2 l$ is the total number of chain units in the crystallite, $\Delta\mu$ is the free-energy difference per chain unit between solid and liquid, and σ_e and σ_l are the surface free energies for the fold surface and the lateral surface, respectively. On the right-hand side of Eq. 19, we can see that there are competing terms: the first one is the thermodynamic driving force for crystallization, and the remaining two terms are the surface free-energy penalties. Accordingly, there are two basic ways to accelerate the polymer nucleation rate, i.e., enhance the driving force or decrease the barrier. An interesting way to enhance the driving force is to decrease the polymer conformational entropy in the liquid through pre-aligning or stretching of the chains under an extensional or shear flow. Under those conditions, one often observes the formation of a stack of lamellae around a central fiber. The resulting morphology has been given the name "shish kebab" [105, 111–114]. The central fiber can be a substrate for the nucleation of lamella growth as in a heterogeneous nucleation. As can be seen in Fig. 10, in simulations even a single pre-aligned chain can facilitate the nucleation of lamellar crystallites, leading to the shish-kebab structure [58]. In this case, the remaining chains in the liquid were not pre-aligned; hence the central fiber acted as a template for the nucleation of lamellar crystals.

The critical size of crystallites can be calculated from the condition $\partial\Delta F(\nu)/\partial\nu = 0$. Beyond the critical size, the thermodynamic condition for crystal growth is $\partial\Delta F(\nu)/\partial\nu \leq 0$. Since at the later stage of crystal growth, $R \gg l$, the last term on the right-hand side of Eq. 19 can be omitted. The thermodynamic growth condition, therefore, gives $l \geq 2\sigma_e/\Delta\mu \equiv l_{min}$. This means that there is a minimum thickness of lamellae for the lateral crystal growth. The linear relationship between l^{-1} and T_m (or T_c) has been observed by small-angle X-ray scattering measurements in many polymer systems [115, 116].

In the classical Lauritzen–Hoffman theory for the mechanism of polymer crystal growth [106], it is assumed that the observed lamellar thickness corresponds to those crystallites that happen to have the largest growth velocity. However, this picture is hard to reconcile with the experimental observation that the thickness of polyethylene single crystals can be modulated by varying the temperature at which they are grown [117, 118]. In fact, simulations by Doye et al. [119, 120] suggest that the observed lamellar thickness does

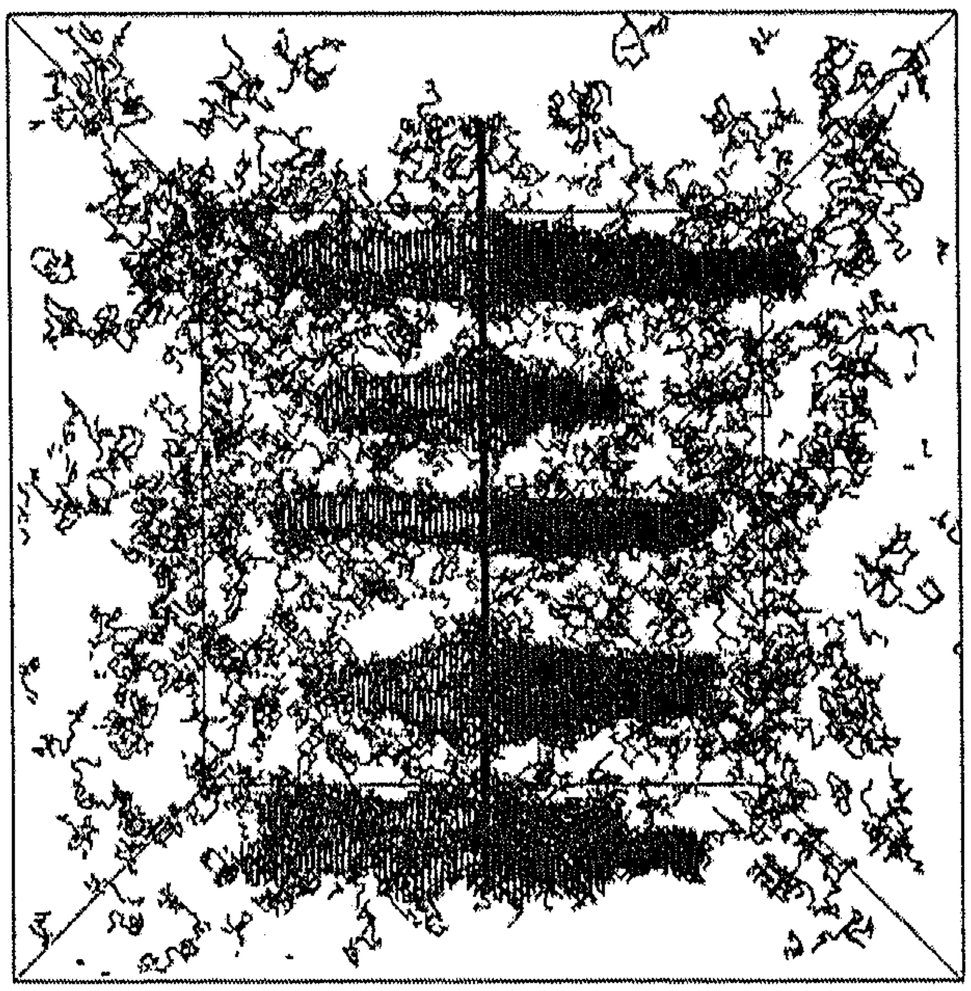

Fig. 10 Snapshot of a shish-kebab crystallite induced by a pre-aligned single chain (drawn much thicker than other chains for better visibility) in a solution. The chain length is 32 units and the thickness of crystallites is about 7 units. The bonds are drawn in *solid cylinders* [58]

not correspond to a maximal growth velocity, but rather to a condition of dynamic stability during growth.

The tip of a growing lamellar crystal has a thickness close to l_{min}. However, behind the tip, the crystallite tends to thicken, as this increases the thermodynamic stability of the crystallite. Whether or not such crystallite thickening occurs depends on the ability of the polymer chains in the crystallites to undergo sliding diffusion [121–123]. High *c*-slip mobility such as what is observed in the hexagonal phase of polyethylene, can even lead to the formation of extended chain crystallites, while low *c*-slip mobility such as is observed in the orthorhombic phase of polyethylene prohibits the "stretching out" of folded-chain crystallites. When the polymer chains are sufficiently short, one can observe that the thickening proceeds in steps: from one state of integral folding to the next [106]. As our dynamic Monte Carlo simulations allow for sliding diffusion, we can study the phenomenon of crystal thickening by simulation. In order to do so, we should take account of the fact that long stems experience more friction during sliding diffusion than short stems. It is possible to account for this length-dependent friction in a way that satisfies detailed balance [57]. Figure 11 shows the thickening from a twice-folded to a once-folded layer for 32-mers.

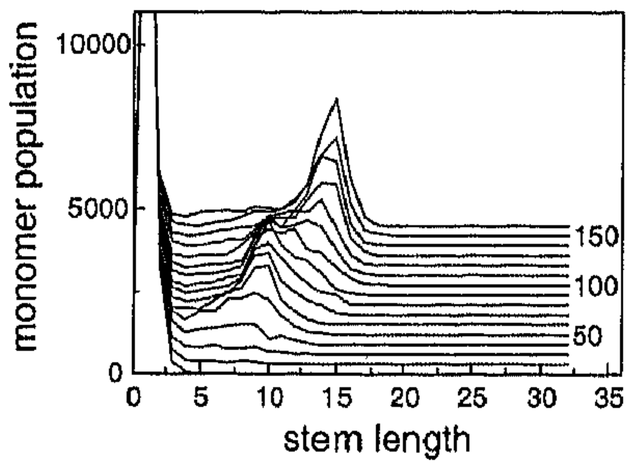

Fig. 11 Monomer distributions of 32-mers with $E_f/E_c = 0.1$ at $E_c/k_B/T = 0.174$ vs. variable crystalline-stem lengths changing with time during isothermal crystallization at a specific temperature. The evolution time is denoted by the *numbers* (times 1000 Monte Carlo cycles) near the curves. The curves are shifted vertically with an interval of 300 for clarity. We can see that with time the peak shifts from one third to half of the chain length [56]

4.2 Crystallization and Melting of Statistical Copolymers

Irregularities in the structure of the polymer backbone will make it difficult for a polymer to be incorporated in a regularly packed crystal structure. This phenomenon is particularly pronounced in systems of random copolymers that consist of a mixture of crystallizable monomers and noncrystallizable comonomers. A very simple way to represent the difference in crystallizability is to assume that crystallizable monomers have a parallel bond–bond interaction energy E_p, while no such interaction is present in pairs of bonds involving the comonomers [52]. In addition, we account for the difference in the size of monomers and comonomers by assuming that the comonomers cannot diffuse through a crystalline region of monomers. With these ingredients, we can perform dynamic Monte Carlo simulations to study how the statistical nature of the copolymers affects the crystal morphology. Three kinds of statistical sequences were then generated, namely, homogeneous (randomly sequenced) copolymers, homogeneous (slightly alternating) copolymers, and heterogeneous (a product in batch reaction with a significant compositional shift) copolymers. On cooling from the melt and then on reheating, crystallization and melting of bulk statistical copolymers were monitored through the absolute crystallinity, which was defined as the fraction of monomer bonds having more than five parallel neighbors of the same type. We find that the phase transition temperatures depend not only on the comonomer content but also on the sequence distribution. Figure 12 shows that on cooling a copolymer system, almost all monomers eventually end up in crystalline domains, irrespective of the composition of the copolymer. Upon reheating a partially crystallized system, we first observe crystallization, rather than melting (cold crystallization). The crystallites that form first upon cooling tend to contain predominantly long monomer sequences. Hence there is

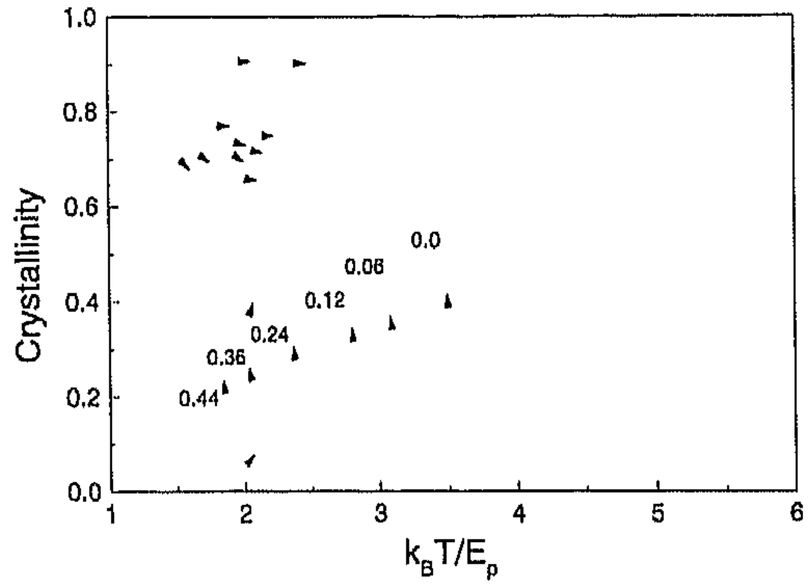

Fig. 12 Cooling (*solid lines*) and heating (*dotted* and *dashed lines*) crystallinity curves of random copolymers with variable comonomer mole fractions as denoted near the curves. The *dashed lines* start from the reduced temperature of 2 and meet the *dotted curves* at high temperatures [52]

a sequence-length segregation during crystallization (Fig. 13) [124]. As the comonomer content of the polymer is increased, the morphology of the crystallites changes from lamellar to granular (Fig. 14). A more detailed analysis can be found in Ref. [52]. Furthermore, there exists a liquid–liquid demixing in the heterogeneous copolymers, but not in the homogeneous copolymers, before the crystallization occurs on cooling (Fig. 15). Since the heterogeneous copolymers are some kinds of polymer blend, the principle of this prior demixing was actually discussed in Sect. 3.3.

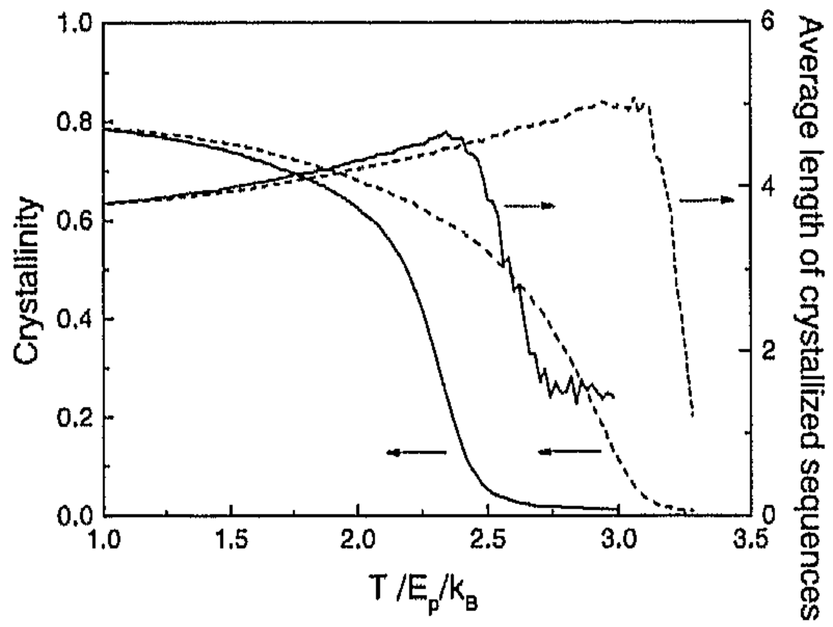

Fig. 13 Cooling (*solid line*) and heating (*dashed lines*) curves of crystallinity and averaged length of crystallized sequences for slightly alternating copolymers with a comonomer mole fraction 0.24. The crystallized sequences are defined as the monomer sequences more than half of whose bonds are in crystalline states [124]

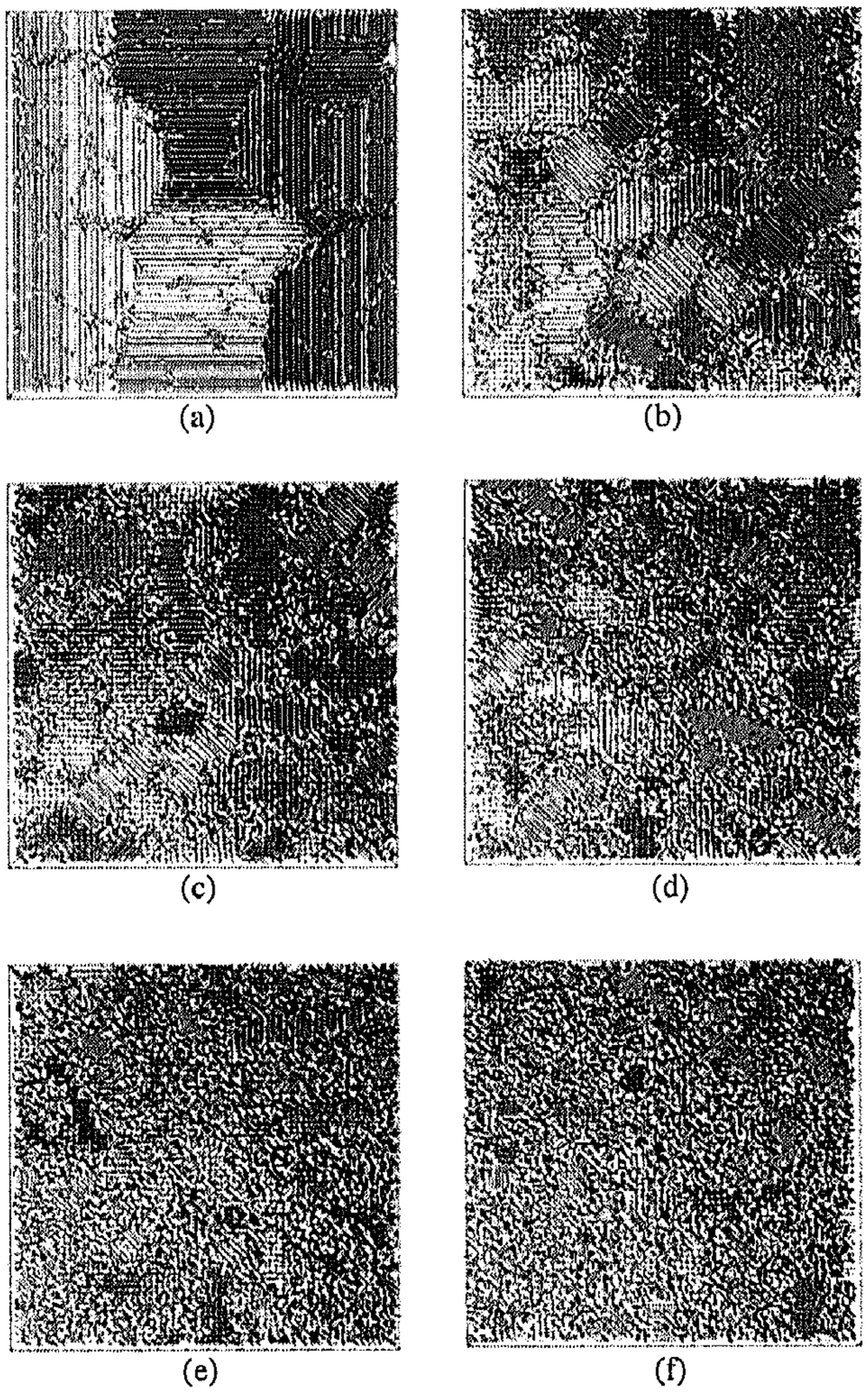

Fig. 14 Snapshots of random copolymers with variable comonomer mole fractions at the reduced temperature of 1 in the cooling process of Fig. 12. a–f Comonomer contents of 0, 0.06, 0.12, 0.24, 0.36, and 0.44, respectively. Polymer bonds are drawn in *cylinders* and the bonds containing comonomers are shown in *double thickness* [52]

4.3 Free-Energy Barrier for Melting and Crystallization of a Single-Homopolymer Model

Thus far, we have been discussing the crystallization of a multichain system. However, under suitable conditions, crystallization can even occur in a single-chain system. Using a combination of biased sampling, multihistogram techniques, and parallel tempering [125], we can directly compute the

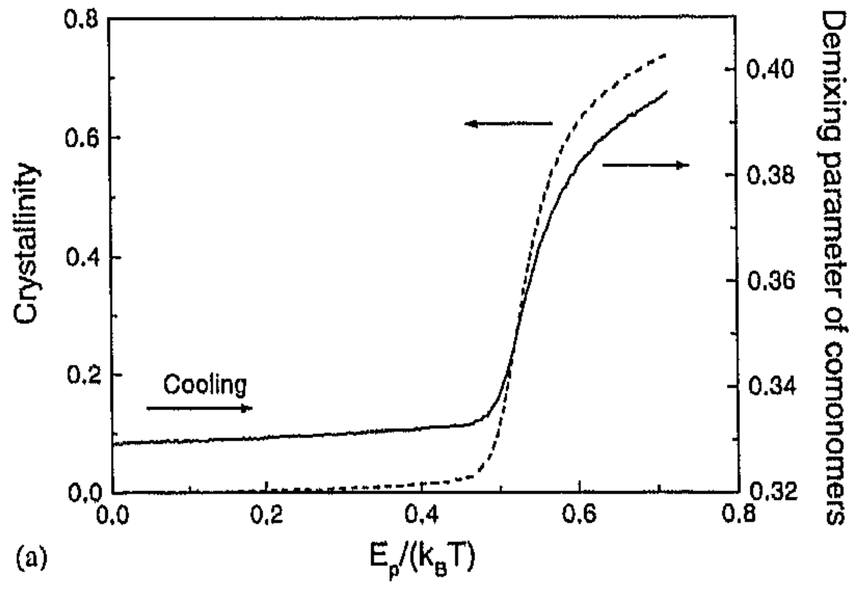

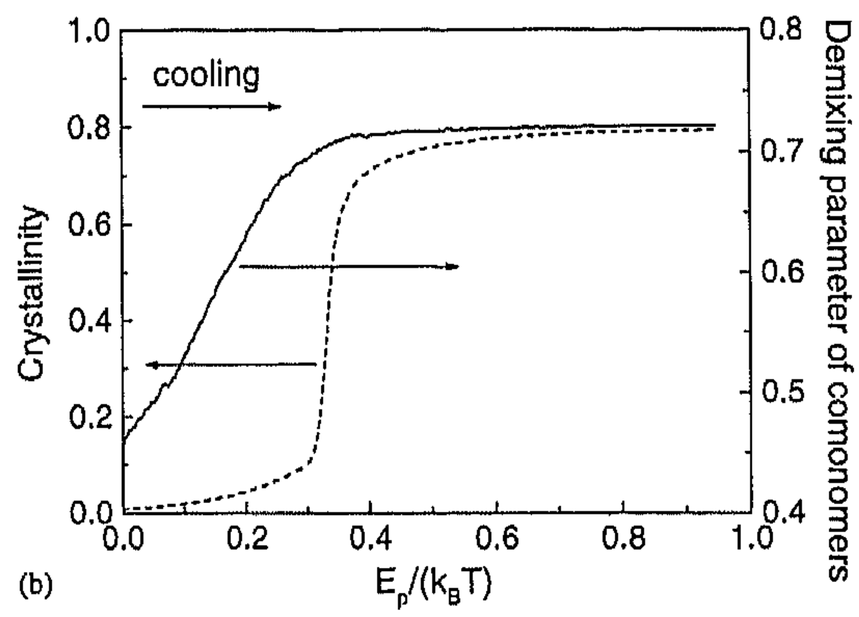

Fig. 15 Cooling curves of crystallinity (*solid line*) and demixing parameter of comonomers (*dashed line*). The latter is defined as the mean fraction of neighboring sites occupied by other comonomers around each comonomer. The cooling program is a stepwise increase of $E_p/(k_BT)$ from zero with a step length of 0.002 and a step period of 300 Monte Carlo cycles. **a** The slightly alternating copolymer with a comonomer mole fraction 0.36; **b** the heterogeneous copolymer with a comonomer mole fraction of 0.36 [52]

free-energy barrier (if any) that separates the crystalline state of the single chain from the disordered "coil" state [126]. Technical details can be found in Sect. A.4. The simulations showed that, at coexistence, there can be a quite high free-energy barrier between the crystalline and molten states of a single chain. The height of this free-energy barrier depends on chain length [127]. As can be seen from Fig. 16, the chain-length dependence can be described by a simple nucleation-like model that takes into account the bulk and surface contributions to the free energy change of single-chain melting:

$$\Delta F_{\mathrm{melt}} = n_{\mathrm{m}} \Delta f_{\mathrm{melt}} + \sigma (N - n_{\mathrm{m}})^{2/3}, \tag{20}$$

where n_{m} is the number of molten units, Δf_{melt} is the free-energy change of each chain unit on melting of bulk polymers, σ represents surface free energy of the crystallite, and N is the chain length.

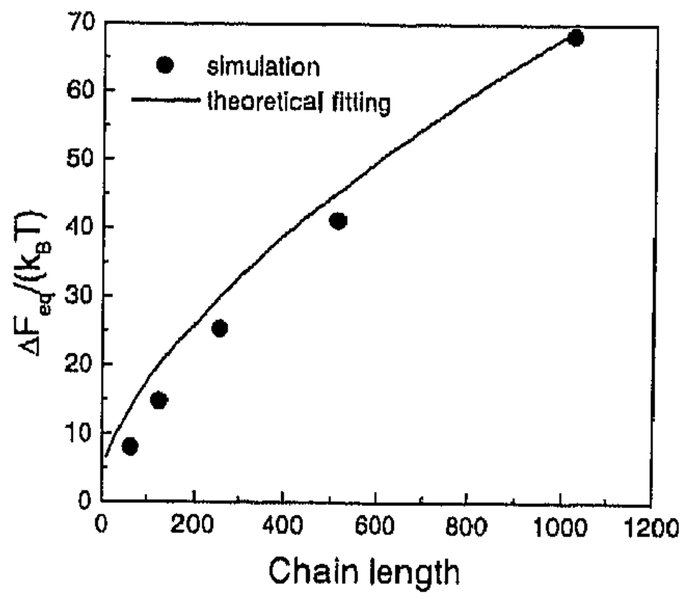

Fig. 16 Height of the equilibrium free-energy barrier for melting and crystallization vs. the chain length in single-chain systems. The *circles* are the simulation results, and the *solid line* is calculated from Eq. 20 with fitting parameter $\sigma = 15E_p$ [127]

Equation 20 predicts a free-energy barrier for primary crystal nucleation (i.e., the free-energy difference between the top of the barrier and the initial coil state) as

$$\Delta F_c = \frac{4\sigma^3}{27\Delta f_{melt}^2}. \tag{21}$$

Interestingly, this barrier does not depend on chain length. This result coincides with experimental observations on the primary nucleation rate of bulk polymers [128–130]. For secondary nucleation of crystallization on a smooth growth front, a similar free-energy expression can be obtained for 2D nucleation:

$$\Delta F_{melt,2D} = n_m \Delta f_{melt,2D} + \sigma_{2D}(N - n_m)^{1/2}, \tag{22}$$

where $\Delta f_{melt,2D}$ and σ_{2D} have slightly different values from Eq. 20. The free-energy barrier for secondary nucleation is still independent of chain length, and is given by

$$\Delta F_{c,2D} = \frac{\sigma^2}{4\Delta f_{melt,2D}}. \tag{23}$$

This result also happens to be compatible with the experimental observations on the crystal growth rate of bulk polymers [131, 132]. In addition, both Eqs. 21 and 23 give a reasonable temperature dependence of the free-energy barriers for primary nucleation and secondary nucleation, compared with the the cases for bulk polymers. It is therefore tempting to speculate that the rate of crystallization of bulk polymers is determined by intramolecular nucleation, similar to the macromolecular nucleation mechanism suggested by Wunderlich [133]. The model suggests that both primary nucleation and secondary nucleation of long-chain polymers are dominated by an intramolec-

ular process. Incidentally, such an intramolecular nucleation model provides a natural explanation for the observed molecular-size fractionation during polymer crystal growth.

The free-energy barrier for melting and crystallization of single chains is also dependent on the quality of the solvent. The same concepts that apply to the interplay of polymer crystallization and liquid–liquid demixing in polymer solutions are also relevant in the freezing of a single-chain system: a large positive B will drive a coil–globule collapse transition [134], while a large E_p drives crystallization [126]. The mean-field theory developed for a polymer solution is still meaningful for the single-chain system. Figure 17 shows that if B/E_p is

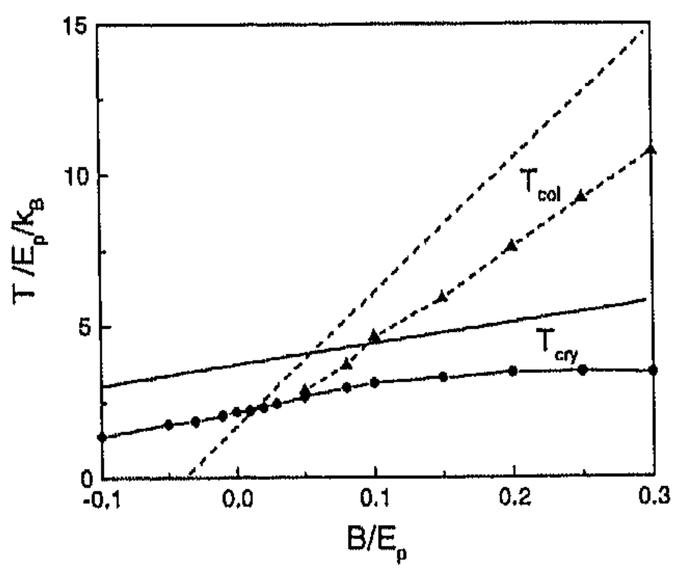

Fig. 17 B/E_p dependence of the critical temperatures of liquid–liquid demixing (*dashed line*) and the equilibrium melting temperatures of polymer crystals (*solid line*) for 512-mers at the critical concentrations, predicted by the mean-field lattice theory of polymer solutions. The *triangles* denote T_{col} and the *circles* denote T_{cry}; both are obtained from the onset of phase transitions in the simulations of the dynamic cooling processes of a single 512-mer. The segments are drawn as a guide for the eye (Hu and Frenkel, unpublished results)

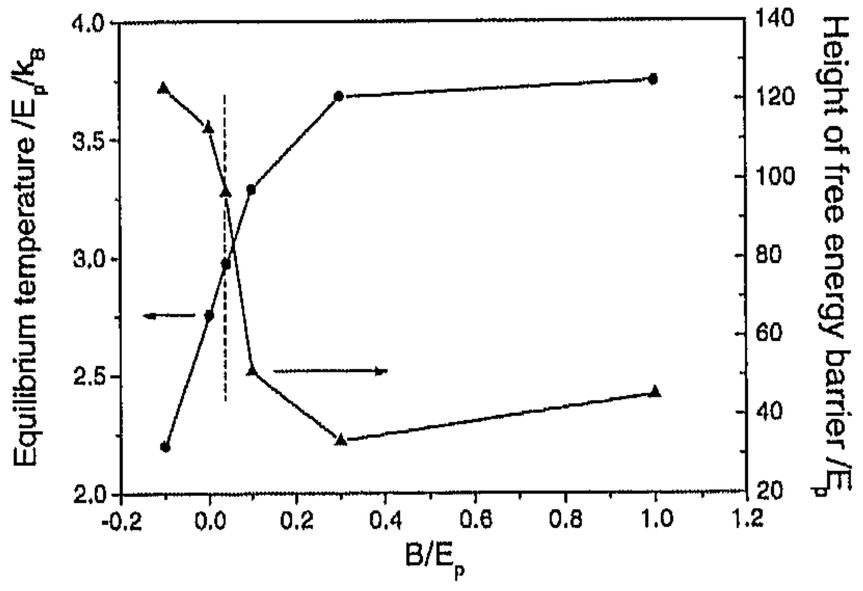

Fig. 18 The equilibrium temperatures (*circles*) and the heights of the free-energy barrier at these temperatures (triangles) for a single 512-mer as a function of B/E_p. The *dashed line* shows the demarcation for the occurrence of a prior collapse transition (Hu and Frenkel, unpublished results)

small (or even negative) there will be a direct transition from the coil state to the single-chain crystal. In contrast, for large positive values of B/E_p a coil–globule transition will precede the transition to the crystalline state (Hu and Frenkel, unpublished results). The free-energy barrier for crystallization decreases with increasing B/E_p, but levels off once there has been a prior coil–globule collapse transition (Fig. 18). These results suggest that single-chain crystallization is easiest if the polymer has undergone a prior coil-to-globule transition, yet the temperature is not so low that the globule has effectively vitrified.

Appendix

A
Dynamic Monte Carlo Simulations of Lattice Polymers

A.1
Microrelaxation Model

In the dynamic Monte Carlo simulations that we describe, polymers "live" on a lattice [135]. They can move either by local jumps or by "sliding" moves that involve a longer stretch of the polymer. The ability to perform such sliding moves greatly increases the rate at which the polymers can sample configuration space. Moreover, it mimics the real dynamics of polymers in dense media. For this reason, the present "microrelaxation model" allows us to gain some insight into the dynamics by which an initial nonequilibrium state of the polymer system relaxes. The first microrelaxation model for lattice polymers was suggested by Verdier and Stockmayer [136], who allowed the change of local chain conformation through end-bond twisting, kink jumping, and crankshaft rotation. The sliding diffusion model was developed to simulate chain diffusion on a lattice [137]. However, all of these models tend to be rather inefficient in changing the orientational distribution of bond vectors, as new bond orientations are predominantly generated at the chain ends. These models are therefore not very efficient in achieving conformational relaxation. In contrast, the kink-generation model allows new bond vectors to be generated in the middle of the chains [138]. This kink-generation model was later developed into the well-known bond-fluctuation model [139, 140]. Actually, combining both kink generation and sliding diffusion together provides higher efficiency for chain relaxation. Such a hybrid approach was first suggested by Lu and Yang [141]. In this hybrid model, sliding diffusion that extends to the end of the chain is allowed during kink generation. In the algorithm that we use, we assume that sliding diffusion takes place between two defects: it is terminated by smoothening out the nearest kink along the chain (Fig. 19) [134]. In this respect, the algorithm is a numerical implementation

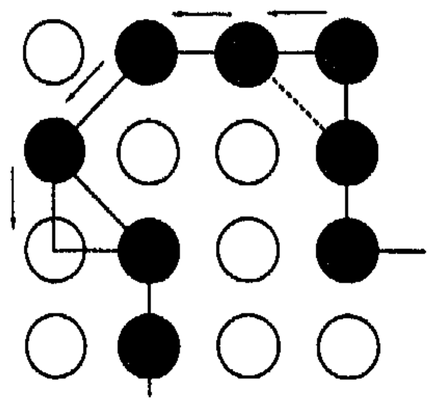

Fig. 19 Our hybrid microrelaxation model. The *solid circles* are occupied by a polymer chain. The *dashed lines* show the new bond positions produced by a move consisting of kink generation and partial sliding diffusion along the chain. The *arrows* indicate the directions of monomer jumping [134]

of the kink-defect diffusion mechanism proposed by de Gennes [142]. Since the polymer bonds are allowed to stay either along the lattice axis or along the body and face diagonals, the coordination number of such a cubic lattice includes all the neighbors along these directions, namely, $6 + 8 + 12 = 26$. In all simulations, we used periodic boundary conditions. In order to map the length and time scales of the lattice model onto those of real polymer systems, one can study the behavior of the radius of gyration (or the end-to-end distance) of the polymer chain (for static properties) and the polymer diffusion coefficient (for dynamics) [143]. Figure 20 shows the mean-square end-to-end distance of lattice polymers vs. the chain length r for polymer solutions over a wide range of concentrations. In very dilute solutions, the polymer size (in three dimensions, in an athermal solvent) is expected to scale as $\langle h^2 \rangle \sim r^{1.2}$, while in the melt, it scales as $\langle h^2 \rangle \sim r$ [144]. Figure 20

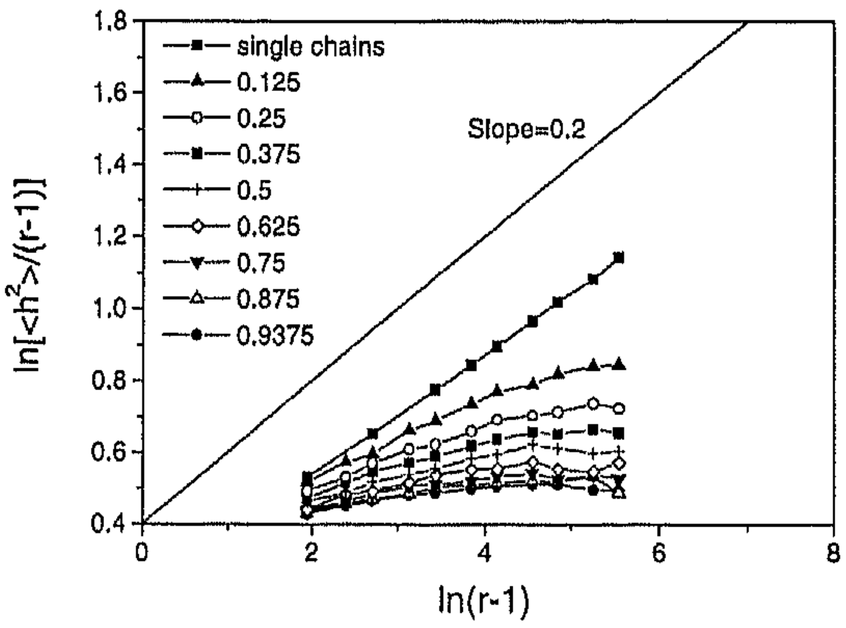

Fig. 20 Mean-square end-to-end distance of chains vs. chain length in a 32 (or above)-sized cubic lattice. The data are those of the polymer volume fractions (Hu and Frenkel, unpublished results)

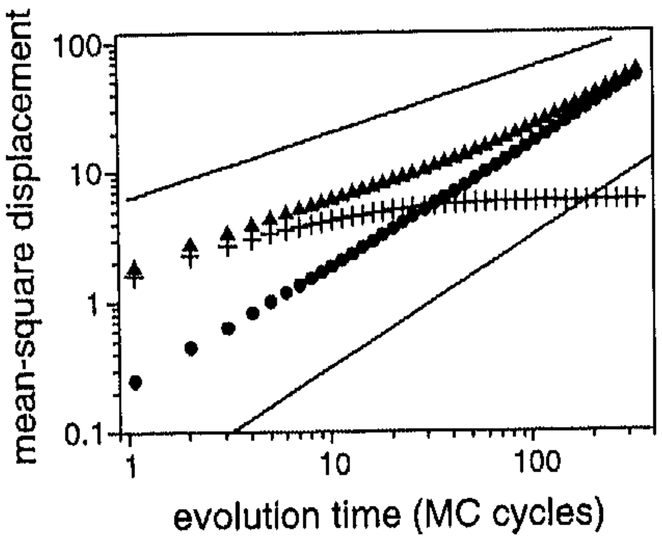

Fig. 21 Mean-square displacement vs. evolution time for 16-mers with an occupation density of 0.9375 in a 32-sized cubic lattice. The *triangles* are for four middle chain units, the *circles* are for the mass center, and the *crosses* are for the chain units relative to the center of mass. The *lines* with slopes of 1.0 and 0.5 indicate the scaling expected according to the Rouse model of polymer chains [56]

shows the slopes of $\ln(\langle h^2 \rangle / r)$ vs. $\ln(r)$ changing from 0.2 to zero with the increase of polymer concentrations. Figure 21 shows the time dependence of the mean-square displacements of individual chain units, of the chain units relative to the mass center, and of the center of chain mass. For the relatively short chains studied, we expect to observe Rouse dynamics [145], as is indeed the case.

A.2 Sampling Strategy

In our simulations, we use the Metropolis method to accept or reject trail moves [146]. Moves are rejected if they cause hard-core overlaps or bond crossing; otherwise, they are accepted with a probability equal to $\min\{1, \exp[-\Delta E/(k_B T)]\}$, where $\Delta E/(k_B T) = (bB + pE_p + cE_c)/(k_B T) = (bB/E_c + pE_p/E_c + c)E_c/(k_B T)$. The meaning of the quantities B, E_p, and E_c is described in the main text, b denotes the change in the number of polymer–solvent contacts, p is the change in the number of nonparallel pairs of neighboring bonds, and c accounts for the change in the number of noncollinear connections between consecutive bonds along the chain. Within the same model, we can add a frictional energy penalty E_f for the local sliding diffusion of chains in the crystalline region. Note that this penalty is present in forward and reverse moves; therefore, it does not affect the detailed balance condition. Rather, it acts like a kinetic pre-factor that slows down the sliding diffusion of long polymer stems in the crystallites, compared with that of short ones [56]. The potential energy barrier can be expressed in the reduced parameters. $k_B T/E_c$ is often used as the reduced temperature, B/E_c is a meas-

ure for the solvent quality, and E_p/E_c reflects the flexibility of the chains. For fully flexible chains, $E_c = 0$. Then, $k_B T/E_p$ is used as the reduced temperature. Usually, we fix $E_p/E_c = 1$ for the semiflexible chains.

A.3 Temperature Scanning Program

To perform temperature scans, we increase/decrease the value of $E_c/(k_B T)$ in steps of size 0.002. Every step takes 300–500 Monte Carlo cycles [14]. In monitoring the properties of the system during heating or cooling, we discard the results of the first 100–400 Monte Carlo cycles because the system is far from equilibrium at the early stages of every step. Statistics on thermal or structural properties of the system are then collected during the remainder of the step. We use the "disorder parameter" described in the main text to monitor the progress of crystallization. To monitor the phase separation, we follow the behavior of the mixing parameter, defined as the mean fraction of solvent sites around a chain unit. To facilitate comparison with experiment, we use the same (rather ad hoc) methods to detect the onset of phase transitions: it is defined as the crossing point of two lines extrapolated from the transition region and from the one-phase region on either side of the phase transition, respectively. To observe primary nucleation on cooling, a large supercooling is usually required. This can delay the onset of crystallization well beyond the equilibrium freezing point, especially in the case of dilute solutions. To suppress such overshooting effects we introduce one molecular layer of solid substrate consisting of fully extended chains. This substrate serves as a template for primary nucleation of both crystallization and liquid–liquid demixing. Figure 22 compares two cooling curves: one was obtained

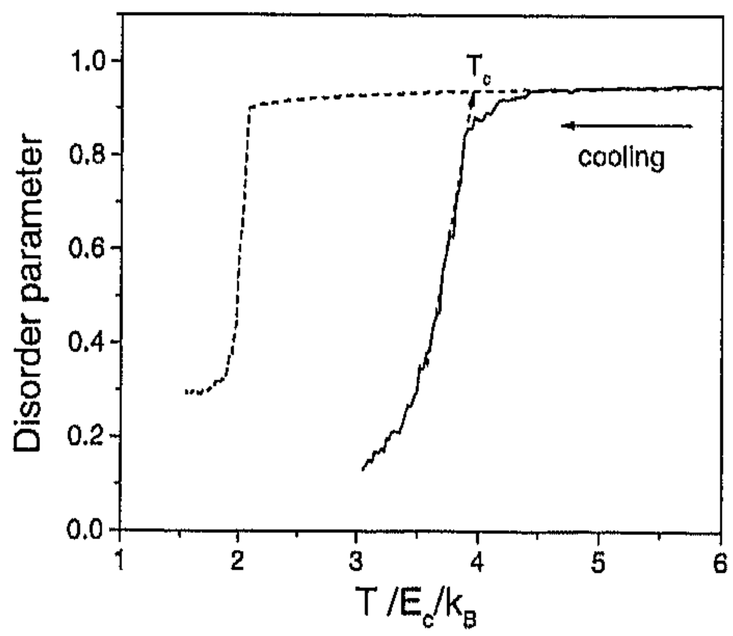

Fig. 22 Cooling curves of the disorder parameter for 32-mers in 32-sized cubic lattice with a conventional cooling program (*dashed line*) and an optimized cooling program (*solid line*). Polymers have a volume fraction of 0.0625 with $B/E_c = 0$ and $E_p/E_c = 1$ [14]

by cooling a homogeneous phase; the other employed the substrate to suppress overshooting. Clearly, the presence of the template significantly raises the onset temperature of crystallization in dilute solutions.

A.4 Biased Sampling and Multihistogram Parallel Tempering

The formation of crystal nuclei in a moderately supersaturated solution is a rare event. In order to probe the frequency of such fluctuations, we used umbrella sampling [148]. In particular, we bias the formation of crystallites by increasing their Boltzmann weight. In fact, during a single simulation, we favor the formation of crystallites with crystallinity x_1 in a window around x_0 by lowering their potential energy with $W = k(x_1 - x_0)^2$, where k determines the width of the window. To recover the free energy of the clusters in the unbiased system, we have to correct for the bias [149, 150]. In practice, about 15 overlapping windows were employed to calculate the free-energy barrier separating the crystalline and disordered states of a single-chain system [126]. The multiple histograms in the simulations of these windows are then merged to form a single, smooth curve. Parallel tempering was used to enhance equilibration between the different windows. An example is shown in Fig. 23.

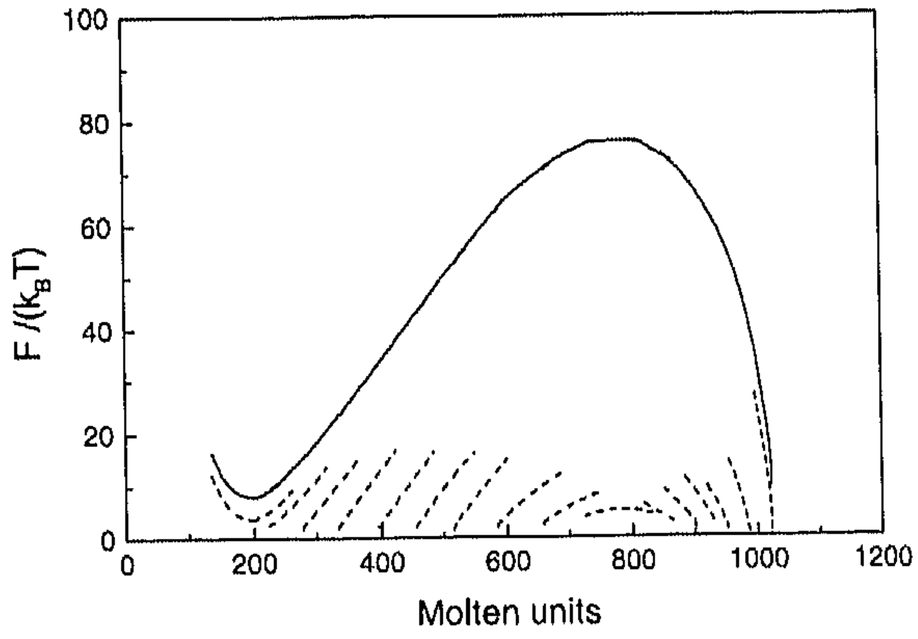

Fig. 23 Parallel tempering of the free-energy curves in the overlapping windows as a function of the number of molten units for a single 1024-mer at a temperature of $2.967E_p/k_B$. The y-axis is not for the absolute value of the free energy but for the relative distribution of the free energy (Hu and Frenkel, unpublished results)

Acknowledgements This work is part of the research program of the Stichting voor Fundamenteel Onderzoek der Materie (FOM), which is financially supported by the Nederlandse organisatie voor Wetenschappelijk Onderzoek (NWO). We thank S. van Albada for critically reading the manuscript. W. H. thanks the funding of National Natural Science Foundation of China (Grant No. 20474027).

References

1. Onsager L (1949) Ann NY Acad Sci 51:627
2. Maier W, Saupe AY (1959) Z Naturforsch 14a:882
3. Maier W, Saupe AY (1959) Z Naturforsch 15a:287
4. Jaehnig F (1979) J Chem Phys 70:3279
5. Ronca G, Yoon DY (1982) J Chem Phys 76:3295
6. Ronca G, Yoon DY (1984) J Chem Phys 80:925
7. ten Bosch A, Maissa P, Sixon P (1983) J Chem Phys 79:3462
8. ten Bosch A, Maissa P, Sixon P (1983) J Phys Lett (Paris) 44:L105
9. Khokhlov AR, Semenov AN (1985) J Stat Phys 38:161
10. Gupta AM, Edwards SF (1993) J Chem Phys 98:1588
11. Lekkerkerker HNW, Vroege GJ (1993) Philos Trans R Soc Lond Ser A 344:419
12. Flory PJ (1956) Proc R Soc Lond Ser A 234:60
13. Hu WB (2000) J Chem Phys 113:3901
14. Hu WB, Frenkel D, Mathot VBF (2003) J Chem Phys 118:10343
15. Rowlinson JS (1970) Faraday Disc Chem Soc 49:30
16. Guggenheim EA (1952) Mixtures. Clarendon, Oxford
17. Flory PJ (1953) Principles of polymer chemistry. Cornell University Press, Ithaca, NY p 495
18. Prigogine I (1957) The molecular theory of solution. North-Holland, Amsterdam
19. Meyer KH (1939) Z Phys Chem B 44:383
20. Huggins ML (1942) Ann NY Acad 43:1
21. Flory PJ (1942) J Chem Phys 10:51
22. Flory PJ (1982) Proc Natl Acad Sci USA 79:4510
23. Nagle JF (1974) Proc R Soc Lond Ser A 337:569
24. Gordon M, Kapadia P, Malakis A (1976) J Phys A 9:751
25. Gujrati PD (1980) J Phys A 13:L437
26. Gujrati PD, Goldstein MJ (1981) J Chem Phys 74:2596
27. Nagle JF, Gujrati PD, Goldstein MJ (1984) J Phys Chem 88:4599
28. DiMarzio EA (1961) J Chem Phys 35:658
29. Ronca G (1983) J Chem Phys 79:6326
30. Jarry JP, Monnerie L (1979) Macromolecules 12:316
31. Doi M, Pearson D, Kornfield J, Fuller G (1989) Macromolecules 22:1488
32. Watanabe H, Kotaka T, Tirrell M (1991) Macromolecules 24:201
33. Baumgaertner A, Yoon DY (1983) J Chem Phys 79:521
34. Yoon DY, Baumgaertner A (1984) Macromolecules 17:2864
35. Boyd RH (1986) Macromolecules 19:1128
36. Mansfield ML (1994) Macromolecules 27:4699
37. Meyer H, Mueller-Plathe F (2002) Macromolecules 35:1241
38. Weber H, Paul W, Binder K (1999) Phys Rev E 59:2168
39. Weber H, Paul W, Kob W, Binder K (1997) Phys Rev Lett 78:2136
40. Baumgaertner A (1984) J Chem Phys 81:484; (1986) J Chem Phys 84:1905
41. Kolinsky A, Skolnick J, Yaris R (1986) Macromolecules 19:2560
42. Weber TA, Helfand E (1979) J Chem Phys 71:4760
43. Fischer EW, Strobl GR, Dettenmaier M, Stamm M, Steidle N (1979) Faraday Disc Chem Soc 68:26
44. Walasek J (1990) J Polym Sci Part B Polym Phys 28:1075
45. Walasek J (1990) J Polym Sci Part B Polym Phys 28:2473
46. Bleha T (1985) Polymer 26:1638

47. Mansfield (1983) Macromolecules 16:914
48. Yoon DY (1989) Polym Prepr Am Chem Soc Div Polym Chem 30:63
49. McCoy JD, Honnell KG, Schweizer KS, Curro JG (1991) J Chem Phys 95:9348
50. van Ruiten J, van Dieren F, Mathot VBF (1993) In: Dosiere M (ed) Crystallization of polymers. Kluwer, Dordrecht, p 481
51. Hu WB, Yu TY (1995) Chem J Chin Univ 16:1140
52. Hu WB, Frenkel D, Mathot VBF (2003) Macromolecules 36:2165
53. Toma L, Toma S, Subirana JA (1998) Macromolecules 31:2328
54. Chen CM, Higgs PG (1998) J Chem Phys 108:4305
55. Hu WB, Yu TY, Bu HS (1994) Chem J Chin Univ 15:1099
56. Hu WB (2001) J Chem Phys 115:4395
57. Hu WB, Frenkel D, Mathot VBF (2003) Macromolecules 36:549
58. Hu WB, Frenkel D, Mathot VBF (2002) Macromolecules 35:7172
59. Lenz RW (1967) Organic chemistry of synthetic high polymers. Interscience, New York, p 91
60. Wunderlich B (1973) Macromolecular physics, vol 1. Crystal structure, morphology, defects. Academic, New York, p 68
61. Tadokoro H (1979) Structure of crystalline polymers. Wiley, New York, p 15
62. Sperling LH (1992) Introduction to physical polymer science, 2nd edn. Wiley, New York, p 261
63. Pan Y, Cao MY, Wunderlich B (1989) In: Brandrup J, Immergut EH (eds) Polymer handbook, 3rd edn. Wiley, New York, p VI/376
64. Bunn CW (1955) J Polym Sci 16:323
65. Wunderlich B (1980) Macromolecular physics, vol 3. Crystal melting. Academic, New York, p 27
66. Mandelkern L (2002) Crystallization of polymers,vol 1, 2nd edn. Equilibrium concepts. Cambridge University Press, Cambridge, p 42
67. Flory PJ, Vrij A (1963) J Am Chem Soc 85:3548
68. Bawendi MG, Freed KF (1988) J Chem Phys 88:2741
69. Buta D, Freed KF, Szleifer I (2000) J Chem Phys 112:6040
70. Richards RB (1946) Trans Faraday Soc 42:10
71. Flory PJ, Mandelkern L, Hall HK (1951) J Am Chem Soc 73:2532
72. He XW, Herz J, Guenet JM (1987) Macromolecules 20:2003
73. Aerts L, Berghmans H, Koningsveld R (1993) Makromol Chem 194:2697
74. Wang H, Shimizu K, Kim H, Hobbie EK, Wang ZG, Han CC (2002) J Chem Phys 116:7311
75. Flory PJ (1949) J Chem Phys 17:223
76. Mandelkern L (2002) Crystallization of polymers,vol 1, 2nd edn. Equilibrium concepts. Cambridge University Press, Cambridge, p 70
77. ten Wolde PR, Frenkel D (1997) Science 277:1975
78. Talanquer V, Oxtoby DW (1998) J Chem Phys 109:233
79. Sear RP (2001) Phys Rev E 63:066105
80. Inaba N, Sato K, Suzuki S, Hashimoto T (1986) Macromolecules 19:1690
81. Lee HK, Myerson AS, Levon K (1992) Macromolecules 25:4002
82. Guenet JM (1996) Thermochim Acta 284:67
83. Berghmans H, de Cooman R, de Rudder J, Koningsveld R (1998) Polymer 39:4621
84. Hu WB, Frenkel D (2004) Macromolecules 37:4336
85. Schaaf P, Lotz B, Wittmann JC (1987) Polymer 28:193
86. Hu WB, Mathot VBF (2003) J Chem Phys 119:10953
87. Dudowicz J, Freed KF, Douglas JF (2002) Phys Rev Lett 88:095503

88. Dudowicz J, Freed KF (1991) Macromolecules 24:5076; 24:5112
89. Clancy TC, Putz M, Weinhold JD, Curro JG, Mattice WL (2000) Macromolecules 33:9452
90. Xu GQ, Clancy TC, Mattice WL (2000) Macromolecules 35:3309
91. Maier RD, Thomann R, Kressler J, Muelhaupt R, Rudolf B (1997) J Polym Sci B Polym Phys 35:1135
92. Haliloglu T, Mattice WL (1999) J Chem Phys 111:4327
93. Thomann R, Kressler J, Setz S, Wang C, Muelhaupt R (1996) Polymer 37:2627
94. Silvestri R, Sgarzi P (1998) Polymer 39:5871
95. Wang ZG, Phillips RA, Hsiao BS (2000) J Polym Sci B Polym Phys 38:2580
96. Lohse D (1986) J Polym Eng Sci 26:1500
97. Yeh GSY, Lambert SL (1972) J Polym Sci A-2 10:1183
98. Ermer H, Thomann R, Kressler J, Brenn R, Wunsch J (1997) Macromol Chem Phys 198:3639
99. Woo EM, Lee ML, Sun YS (2000) Polymer 42:883
100. Keller A (1957) Philos Mag 2:1171
101. Fischer EW (1957) Z Naturforsch 12a:753
102. Till PH Jr (1957) J Polym Sci 24:301
103. Lindenmeyer PH (1963) J Polym Sci C 1:5
104. Geil PH (1963) Polymer single crystals. Wiley-Interscience, New York
105. Wunderlich B (1973) Macromolecular physics, vol 1. Crystal structure, morphology, defects. Academic, New York, pp 178–379
106. Bassett DC (1981) Principles of polymer morphology. Cambridge University Press, London
107. Welch P, Muthukumar M (2001) Phys Rev Lett 87:218302
108. Lotz B (1994) Philos Trans R Soc Lond Ser A 348:19
109. Bu Z, Cheng SZD, Putthanarat S, Eby RK, Reneker DH, Lotz B, Magonov S, Hsieh ET, Johnson TW, Geerts RG, Plackal SJ, Hawley GR, Welch MB (2000) Macromolecules 33:6861
110. Kelton KF (1991) In: Ehrenreich H, Turnbull D (eds) Crystal nucleation in liquids and glasses. Academic, Boston, p 75
111. Pennings AJ (1977) J Polym Sci Polym Symp 59:55
112. McHugh AJ (1982) Polym Eng Sci 22:15
113. Barham PJ, Keller A (1985) J Mater Sci 20:2281
114. Keller A, Odell JA (1985) Colloid Polym Sci 263:181
115. Al-Hussein M, Strobl G (2002) Macromolecules 35:1672
116. Heck B, Strobl G, Grasruck M (2003) Eur Phys J E 11:117
117. Bassett DC, Keller A (1961) Philos Mag 6:1053
118. Dosiere M, Colet M, Point JJ (1986) In: Sedlacek B (ed) Morphology of polymers. De Gruyter, Berlin, p 171
119. Doye JPK, Frenkel D (1998) Phys Rev Lett 81:2160
120. Doye JPK, Frenkel D (1999) J Chem Phys 110:7073
121. Hikosaka M (1987) Polymer 28:1257
122. Hikosaka M (1990) Polymer 32:458
123. Hikosaka M, Rastogi S, Keller A, Kawabata H (1992) J Macromol Sci Phys B31:87
124. Hu WB, Mathot VBF (2004) Macromolecules 37:673
125. Frenkel D, Smit B (2002) Understanding molecular simulations, 2nd edn. Academic, San Diego, p 167
126. Hu WB, Frenkel D, Mathot VBF (2003) J Chem Phys 118:3455
127. Hu WB, Frenkel D, Mathot VBF (2003) Macromolecules 36:8178

128. Nishi M, Hikosaka M, Ghosh SK, Toda A, Yamada K (1999) Polym J 31:749
129. Ghosh SK, Hikosaka M, Toda A (2001) Colloid Polym Sci 279:382
130. Umemoto S, Hayashi R, Kawano R, Kikutani T, Okui N (2003) J Macromol Sci B 42:421
131. Umemoto S, Okui N (2002) Polymer 43:1423
132. Umemoto S, Kobayashi N, Okui N (2002) J Macromol Sci B 41:923
133. Mehta A, Wunderlich B (1974) J Polym Sci Polym Phys Ed 12:255
134. Hu WB (1998) J Chem Phys 109:3686
135. Kremer K, Binder K (1988) Comput Phys Rep 7:259
136. Verdier PH, Stockmayer WH (1962) J Chem Phys 36:227
137. Wall FT, Mandel F (1975) J Chem Phys 63:4592
138. Larson RG, Scriven LE, Davis HT (1985) J Chem Phys 83:2411
139. Carmesin I, Kremer K (1988) Macromolecules 21:2819
140. Deutsch HP, Binder K (1991) J Chem Phys 94:2294
141. Lu JM, Yang YL (1993) Sci Chin A 36:357
142. de Gennes PG (1971) J Chem Phys 55:571
143. Binder K (1995) In: Binder K (ed) Monte Carlo and molecular dynamics simulations in polymer science. Oxford University Press, New York, p 22
144. de Gennes PG (1979) Scaling concepts in polymer physics. Cornell University Press, Ithaca, NY, p 29
145. Kremer K, Grest GS (1990) J Chem Phys 92:5057
146. Metropolis N, Rosenbluth AW, Rosenbluth MN, Teller AH, Teller E (1953) J Chem Phys 21:1087
147. Binder K (1979) In: Binder K (ed) Monte Carlo methods in statistical physics. Springer, Berlin Heidelberg New York, p 1
148. Torrie GM, Valleau JP (1974) Chem Phys Lett 28:578
149. ten Wolde PR (1998) PhD thesis, Amsterdam University, p 72
150. Auer S, Frenkel D (2001) Nature 409:1020